Human MuStem cell grafting into infarcted rat heart attenuates adverse tissue remodeling and preserves cardiac function hMuStem cells preserve function of infarcted heart

Alice Rannou, Gilles Toumaniantz, Thibaut Larcher, Isabelle Leroux, Mireille Ledevin, Agnès Hivonnait, Candice Babarit, Romain Fleurisson, Laurence Dubreil, Séverine Ménoret, et al.

Human MuStem cell grafting into infarcted rat heart attenuates adverse tissue remodeling and preserves cardiac function

hMuStem cells preserve function of infarcted heart

Authors: Alice Rannou[1,2,3], Gilles Toumaniantz[2,3], Thibaut Larcher[1], Isabelle Leroux[1], Mireille Ledevin[1], Agnès Hivonnait[2], Candice Babarit[1], Romain Fleurisson[1], Laurence Dubreil[1], Séverine Ménoret[4], Ignacio Anegon[4], Flavien Charpentier[2,5,*,†], Karl Rouger[1,*,†], Laetitia Guével[1,3†]

Affiliations:

[1]PAnTher, INRA, École nationale vétérinaire, agro-alimentaire et de l'alimentation Nantes-Atlantique (Oniris), Université Bretagne Loire (UBL), Nantes, F-44307, France.

[2] l'institut du Thorax, INSERM, CNRS, UNIV Nantes, France.

[3]Université de Nantes, Nantes, France.

[4]UMR 1064/core facility TRIP/Nantes Université, CHU Nantes, INSERM, CNRS, SFR Santé, INSERM UMS 016, CNRS UMS 3556, F-44000 Nantes, France.

[5]l'institut du thorax, CHU Nantes, Nantes, France.

*To whom correspondence should be addressed: karl.rouger@inra.fr; flavien.charpentier@univ-nantes.fr

†Equal contribution to this work

Abstract:

Myocardial infarction is one of the leading causes of mortality and morbidity worldwide. While transplantation of several cell types into the infarcted heart has produced promising preclinical results, clinical studies using analogous human cells have shown limited structural and functional benefits. In Dog and Human, we have described a type of muscle-derived stem cells termed MuStem cells that efficiently promoted repair of injured skeletal muscle. Enhanced survival rate, long-term engraftment, and participation in muscle fiber formation were reported, leading to persistent tissue remodeling and clinical benefits. Considering these features that are restricted or absent in cells tested so far for myocardial infarction, we wanted to investigate the capacity of human MuStem cells to repair infarcted heart. Their local administration in immunodeficient rats 1 week after induced infarction resulted in reduced fibrosis and increased angiogenesis 3 weeks post-transplantation. Importantly, foci of human fibers were detected in the infarct site. Treated rats also showed attenuated left ventricle dilation and preservation of contractile function. Interestingly, no spontaneous arrhythmias were observed. Our findings support the potential of MuStem cells, which have already been proposed as therapeutic candidates for dystrophic patients, to treat myocardial infarction and position them as attractive tool for muscle regenerative medicine.

Keywords: Cell therapy, myocardial infarction, human adult stem cell, MuStem cells, regenerative medicine

Introduction

The heart lacks the intrinsic ability to repair damage caused by severe injuries, such as myocardial infarction (MI) [1,2]. Intramyocardial transplantation of stem/progenitor cells constitutes a promising approach to restore cardiac function and prevent progression to heart failure [3]. Preclinical studies conducted over the past 2 decades have evaluated the regenerative potential of multiple cell types. These include myoblasts [4–6], bone marrow mononuclear cells [7,8], mesenchymal stem cells (MSCs) [9,10], and endogenous cardiac progenitors such as c-kit$^+$ cardiac progenitor cells (CPCs) [11], sca1$^+$ CPCs [12], and cardiosphere-derived cells [13], as well as embryonic stem cells [14,15] and induced pluripotent stem cells (iPSC)-induced cardiomyocytes (CMs) [16,17]. Decreased myocardial fibrosis, neovascularization, prevention of left ventricle (LV) dilation, and enhancement of local cardiac contractility have been successively described for stem cells of different origins [18–20], leading to rapid progression to clinical trials for a subset of these cell types. To date however, these encouraging preclinical findings have not been replicated in a clinical setting, and randomized clinical trials for MI have shown only modest long-term efficacy [21], mainly due to poor survival and engraftment of injected cells in the harsh cardiac environment and negligible direct differentiation of stem cells into CMs and/or vascular cells [22,23].

A type of murine muscle-derived stem cells (MDSCs) isolated on the basis of an initial adhesion defect have been shown to implant into infarcted zone, induce neo-angiogenesis and significantly improve cardiac function after transplantation into the hearts of adult immunodeficient mice with acute MI [24]. These outcomes were much better than those obtained with myoblasts, which when transplanted into small and large animal models were associated with poor retention, arrhythmias, and limited spreading from the injection site [25–27]. In recent years, we have isolated and characterized a type of MDSC (MuStem cells) from healthy canine skeletal muscle, and have demonstrated their therapeutic potential after intramuscular and systemic delivery in the Golden Retriever Muscular Dystrophy (GRMD) dog [28]. In this clinically relevant animal model of Duchenne Muscular Dystrophy, MuStem cells show improved survival and greater potential than myoblasts for implantation into severely

damaged tissue, as well as the potential to contribute to long-term myofiber regeneration, satellite cell replenishment, and restriction of fibrosis. Through signaling mediated by several biological pathways, MuStem cell implantation limits the progression of muscle damage and stabilizes the clinical status of recipient dogs [29–31]. More recently, we isolated the human counterpart of MuStem cells (hMuStem cells), for which we have demonstrated comparably robust muscular regeneration capacity after delivery into injured skeletal muscle in immunodeficient mice [32]. These compelling findings point to hMuStem cells as attractive candidates for the treatment of skeletal muscle diseases. Given the positive results obtained following murine MDSC implantation in allogeneic MI models, as well as the specific properties of MuStem cells, which may help overcome the key limitations advanced to explain the limited successes with other cell types tested for the treatment of MI, it is of particular interest to characterize the behavior of hMuStem cells in the context of MI.

Here, we report for the first time the transplantation of hMuStem cells in an immunodeficient rat model of MI. We provide an extensive histological and molecular analysis of their behavior 3 weeks after local administration by considering the post-transplantation survival, engraftment and differentiation of hMuStem cells. Cardiac tissue and functional remodeling was investigated through analysis of the cardiomyogenic, fibrotic and angiogenic compartments as well as the ECG and echocardiography parameters. Overall, we demonstrate the potential of hMuStem cells to counteract adverse cardiac tissue remodeling and preserve cardiac function, suggesting that they could represent a valuable therapeutic tool for the treatment of cardiac diseases, in addition to their demonstrated benefits in the treatment of injured skeletal muscle.

Results

hMuStem cells correspond to early-myogenic progenitors uncommitted to the cardiac lineage

To characterize the hMuStem cell populations used in the transplantation protocol, 4 independent cell batches expanded at passage (P) 5 under good manufacturing practice-like conditions were tested for a panel of lineage-specific markers. In agreement with our previous findings [32,33], flow cytometry revealed that more than 71% of *in vitro*-expanded cells expressed the canonical satellite cell and myoblast marker CD56 [34], while all cells were robustly positive for the recently identified satellite cell markers CD29, CD82, and CD318 [35–37] (Figure 1A). Moreover, the typical MSC markers CD73, CD90, and CD105 were uniformly detected in hMuStem cells that were concomitantly negative for the classical hematopoietic stem cell marker CD45. Three out of 4 cell batches contained 2-6% of cells positive for CD271 (Nerve Growth Factor Receptor), a marker for MSC precursors in bone marrow (representative profile is shown in Figure S1, top left), whereas 44% of $CD271^+$ cells was determined in the other cell batch (Figure S1, bottom left). Co-labeling with CD271 and CD105 evidenced that $CD271^+$ cells were quite all $CD105^+$ (Figure S1, right). hMuStem cells showed homogeneous expression of the well-described perivascular cell markers CD140b and CD146. RT-qPCR analysis to detect cardiac-lineage markers revealed a lack of expression of the well known early transcriptional factors *NK2 Homeobox 5* (*NKX2.5*) and *T-box5* (*TBX5*), as well as *ryanodine receptor-2* (*RYR2*) in all hMuStem cell batches (Figure 1B). Other classical markers, including *voltage-gated sodium channel α-subunit 5* (*SCN5A*) and *troponin T2* (*TNNT2*), were expressed at low levels. Only *gap junction protein α1* (*GJA1*) gene encoding *connexin 43* (*Cx43*), which is required to establish intercellular connections between cardiomyocytes and is also expressed by other progenitor cells such as MSCs [38–40], was detected in hMuStem cells. In addition, a large amount of the phosphorylated isoform of Cx43, which is involved on the electrical cell-to-cell coupling through its action on the gap junction function, was detected by western blotting on hMuStem cells compared to those obtained in proliferating myoblasts

known to express Cx43 (Figure 1C). Taken together, these results indicate that cultured hMuStem cells are early myogenic progenitors with a perivascular/mesenchymal signature that do not exhibit any intrinsic cardiac lineage commitment in their native condition.

Skeletal hMuStem cells can engraft and persist in healthy myocardium

We sought to determine whether hMuStem cells derived from skeletal muscle could be implanted into heart tissue. hMuStem cells were delivered into 6 sites within the mid-portion of the LV of 9 immunodeficient rats. Functional and histopathological studies were performed 3 weeks after stem cell administration, as shown in the schematic in Figure 2A. The extent of hMuStem cell engraftment was also analyzed by immunohistochemistry using an anti-human lamin A/C antibody (Ab) that does not cross-react with rodents. The presence of human cells was confirmed by detection of large clusters of lamin A/C^{+} nuclei in all injected hearts. DAPI counterstaining of the lamin A/C^{+} nuclei showed no change in nucleus appearance typically corresponding to pyknosis, karryorrhexia, and chromatin condensation, indicating that the transplanted hMuStem cells correspond to intact cells. These cells, which were visualized by wheat germ agglutinin (WGA) labeling [41], were mainly randomly scattered throughout the connective tissue, and rarely observed in myocardial tissue (Figure 2B). Also, they correspond to small cells with a poorly developed cytoplasm and harboring only one nucleus (Figure 2B, insert). Topographic hematoxylin-eosin-saffron (HES) staining confirmed that these cells had either very scant, barely visible cytoplasm or a moderate amount of eosinophilic cytoplasm around a large, paracentral euchromatic nucleus (Figure 2C). Activated macrophages were not detected close to the hMuStem cells, as expected in this immunodeficient rat model characterized by a drastic reduction of monocytes and macrophages [42]. Picrosirius staining confirmed that these cells were primarily localized in dense connective tissue. The number of hMuStem cells was estimated using Alu-based technique for detecting human genomic DNA (hDNA) [43]. Non-infarcted hearts retained 16,600-

139,390 cells, depending on the rat, corresponding to 1-5% of the total number of cells originally transplanted. By contrast, samples from the liver, lung, spleen, brain, kidney, and skeletal muscle were all negative for hDNA (data not shown).

Analyses were performed to rule out the presence of electrical, structural, or contractile cardiac dysfunction associated with the persistence of hMuStem cells in injected hearts. ECG analysis revealed no electrical abnormalities (Figure 2D, Table 1 and Table S1). Similarly, the presence of hMuStem cells had no effect on heart rate, atrial (P wave duration), atrio-ventricular (PR interval), or ventricular (QRS complex duration) conduction, or ventricular repolarization (QT interval). Measurement of the left ventricular end-diastolic diameter (LVEDD) and end-diastolic wall thickness (LVEDWT) using M-mode echocardiography revealed no structural remodeling and no alterations in LVEDD (7.22 ± 0.27 mm and 7.43 ± 0.23 mm at baseline and 3 weeks post-injection, respectively) or LVEDWT (1.63 ± 0.07 mm and 1.73 ± 0.08 mm, respectively; Figure 2D, Table 1, and Table S2). Furthermore, we observed no change in systolic function, as assessed by determination of ejection fraction (EF): EF = $84\% \pm 3\%$ and $87\% \pm 2\%$ at baseline and 3 weeks post-injection, respectively). Similarly, we observed no change in diastolic markers (Figure S2), *i.e.,* E/A ratio (E/A = 1.68 ± 0.12 and 1.50 ± 0.08 at baseline and 3 weeks post-injection, respectively), Doppler-derived deceleration time (DT = 39 ± 2 and 44 ± 4 ms, respectively), or isovolumetric relaxation time (IVRT = 27 ± 0.5 and 26 ± 0.9 ms, respectively). These data demonstrate the absence of cardiac structural remodeling or functional alterations 3 weeks after myocardial hMuStem cell transplantation, and indicate that hMuStem cells are capable of engrafting in uninjured hearts without inducing structural remodeling or causing adverse effects on electrical, systolic, or diastolic function.

hMuStem cells attenuate the infarction-induced adverse left ventricular remodeling

To investigate the potential of hMuStem cells to induce cardiac repair in the context of MI, we designed a protocol for cell transplantation in female immunodeficient rats that had undergone permanent occlusion of the left anterior descending (LAD) coronary artery 1 week earlier. Transplantation was followed by functional and histopathological examinations as outlined in the schematic shown in Figure 3A. The coronary ligature caused a 19.79% ± 1.93% reduction in LV ejection fraction (LVEF) after 1 week, indicating induction of moderate MI. One week post-infarction, 20 rats were blindly randomized to receive injections of either 2.7×10^6 hMuStem cells (treated group) or vehicle (mock group) into the infarct border zone. Three weeks post-injection, rats were sacrificed and their LV transversely sectioned from the apex to the base. Depending on the experiment planned, all or half of the sections were frozen and/or embedded in paraffin (Table S3). In the mock group, analysis of HES-stained sections confirmed MI, as evidenced by extensive areas of remodeling and an irregular shape resulting in multiple foci of varying size within the section (Figure 3B). These areas displayed a similar organization that could be divided in two parts: a central zone and a border zone. The central zone was characterized by a complete loss of CMs, which had been replaced by fibrotic tissue rich in collagen, as confirmed by saffron staining, with large fibroblasts displaying a euchromatic nucleus and infiltrated with mixed inflammatory cells. An irregular boundary-demarcated border zone, 30-70 µm thick, surrounded the central area and was mainly composed of hyper-eosinophilic ovoid CMs with marked anisocytosis, individually surrounded by thick bundles of collagen-rich connective tissue. At the periphery of the infarct, viable myocardium retained an organized structure with clearly intact cells. The central zone in all rats in the treated group was much smaller than that of the mock group. Moreover, the border zone in treated rats was thinner than that of vehicle-treated counterparts, or in some cases completely absent, with normal CMs directly adjacent to the central zone.

Fibrotic tissue accounted for 12.6% ± 2.9% and 9.4% ± 1.8% of the entire section in the mock and treated groups, respectively, indicating a trend towards a global decrease in fibrosis following hMuStem cell treatment (Figure 3C). The number of fibrotic foci within the infarct was 14.4 ± 1.2 and

7.6 ± 2.8 in the mock and treated groups, respectively ($p = 0.059$, Mann-Whitney test), indicating that hMuStem cell administration mitigated the development of myocardial fibrosis. Comparison of the infarct and peripheral (*i.e.,* viable) zones revealed that fiber size was more heterogeneous and globally increased in the infarct zone. Fiber size was measured and expressed as the minimal Ferret diameter (Figure 3D). One-way ANOVA revealed a difference in fiber size between zones ($p < 0.001$), but no effect of treatment (vehicle versus hMuStem cells). The size distribution of fibers in the infarct zone is depicted in Figure 3E. Marked anisocytosis was confirmed in rats in both the mock and treated groups. Strikingly, some small fibers (< 5 µm in diameter) were exclusively identified in the treated group.

Revascularization of the heart by the formation of new vessels is one of the preferred therapeutic approaches for MI. Capillary density within the infarct was assessed by von Willebrand factor (vWF) labeling of endothelial cells, while the conjunctive frame was labeled with the WGA. In the mock group, the central MI zone was characterized by the presence of dense WGA^+ areas with a low density of blood capillaries and a few larger blood vessels. Conversely, in the border zone, capillaries were more numerous and had a dilated lumen delineated by large endothelial cells (Figure 4A). The vWF^+ surface accounted for 16.13% ± 5.32%, 7.46% ± 1.81%, and 5.87% ± 1.82% of the infarct, border, and viable zones, respectively, in the mock group (Figure 4B), and for 32.83% ± 4.52%, 18.30% ± 3.64%, and 9.60% ± 0.56% of the corresponding zones in the treated group. There was a 2-fold and 2.5-fold increase in vWF^+ structure in the infarct and border zones, respectively, in the treated versus the mock group, indicating an increased density of capillaries in both zones following hMuStem cell administration ($p < 0.001$). No such differences between groups were observed in the viable zone. These findings indicate that hMuStem cell transplantation induced an angiogenic effect in infarcted hearts by promoting host angiogenesis not only in the border zone, where vascular structures are typically preserved, but also in the infarct zone, in which blood vessels are typically absent. Taken together, our results show that hMuStem cell administration induces profound remodeling of the infarcted heart by acting on cardiomyogenic, fibrotic, and angiogenic compartments.

hMuStem cells engraft into infarcted tissue

Post-transplantation survival of stem/progenitor cells is considered a crucial determinant of the long-term efficacy of transplantation protocols. We therefore investigated whether the beneficial effects observed after hMuStem cell administration were associated with colonization of the injured heart by human cells. Three weeks post-implantation, hMuStem cells populated the infarct of all rats from the treated group (Figure 5A). Foci composed of 15 to over 300 large lamin A/C$^+$ nuclei per section were detected throughout the entire depth of the infarct. Topographic HES staining showed that cells containing lamin A/C$^+$ nuclei displayed either very scant, barely visible cytoplasm or a moderate amount of eosinophilic cytoplasm around the paracentral nucleus. The presence of lamin A/C$^+$ nuclei in the WGA$^+$ area on confocal microscopy showed that most cells were located inside the fibrotic infarct zones (Figure 5A). Few donor cells were observed within the viable host myocardium. Quantitative analysis revealed that 98.5% of donor nuclei were located within the infarct zone, while 1.0% and 0.5% were located in the border and viable zones, respectively, suggesting that hMuStem cells concentrated in the acute infarct zone despite their initial injection in the border zone. To further confirm the retention of transplanted hMuStem cells, the LV of 3 rats from the treated group was analyzed to detect human Alu sequences on genomic DNA extraction. At 3 weeks post-injection, 7 hMuStem cell-treated rats were analyzed by qPCR and cardiac sections from 3 representative rats were assessed to determine the tissue distribution of hMuStem cells. Genomic hDNA analyses identified 93,400-153,820 cells, indicating that 4-5.7% of transplanted cells remained in rats injected with hMuStem cells. By contrast, samples from liver, lung, spleen, brain, kidney and muscle were all negative for hDNA in the treated rats at this time-point (data not shown).

Analysis of cell behavior showed that 1% of donor nuclei expressed proliferating cell nuclear antigen (PCNA), indicating persistence of donor cell proliferation *in vivo* 3 weeks after transplantation

(Figure 5B). Moreover, less than 1% of cells containing lamin A/C$^+$ nuclei were positive for TUNEL, demonstrating that quite all implanted donor cells are not apoptotic cells, and rather correspond to resident cells in the quiescent state. Next, we tracked the fate of hMuStem cells by examining their *in vivo* differentiation potential (Figure 5C-F). Fluorescent co-immunolabeling for human lamin A/C and either the fast skeletal myosin heavy chain (MHC) isoform, the slow skeletal troponin T1 (TNNT1) isoform, or cardiac troponin I (TNNI) showed that a proportion of the transplanted hMuStem cells contributed to the formation of fast or slow skeletal muscle fibers as well as cardiac fibers. As observed in HES-stained sections, these human nuclei-containing fibers colonized the connective tissue with occasional clusters of skeletal muscle fibers. By contrast, human TNNI$^+$ fibers appeared isolated in the fibrotic zone. Fibers positive for skeletal MHC and TNNT1 isoforms accounted for 18% and 19% of fibers respectively, while 5% expressed the TNNI isoform. Even though the Cx43 protein is detected in cultured hMuStem cells, none of the human TNNI$^+$ fibers expresses it, indicating an absence of electrical cell-to-cell coupling with host cardiomyocytes (data not shown). Histomorphometry of skeletal and cardiac fibers showed minimal Feret diameters of 9.01 ± 5.2 µm and 13.53 ± 8.3 µm, respectively, corroborating the aforementioned detection of small fibers in the infarct zone of rats from the treated group. These data show that about 42% of the hMuStem cells that survived after myocardial administration differentiated towards a skeletal myogenic lineage or, to a lesser extent, a cardiac phenotype. Importantly, we observed no hybrid fibers (*i.e.*, those containing both human skeletal and cardiac markers). Lamin A/C$^+$ nuclei were observed sporadically in cells positive for alpha-smooth muscle actin (α-SMA) labeling, although not in all rats, indicating that some hMuStem cells differentiated into myofibroblasts (Figure 5G). Finally, we detected muscle fibers containing several lamin A/C$^+$ nuclei, indicating that hMuStem cells primarily fused with one other when injected into the heart (Figure 5H). Overall, these results show that hMuStem cells have the potential to remain in the infarcted heart with a multifocal presence throughout the depth of the infarct, locating mainly in the

acute fibrotic zone where they contribute to the formation of skeletal and cardiac muscle fibers or constitute resident cells in the connective matrix.

hMuStem cells preserve cardiac function in the infarcted heart

Four weeks after infarction, electrocardiography revealed ST segment depression in lead I in rats from both mock and treated groups (Figure 6A). As observed in the sham-operated rats, engraftment of hMuStem cells caused no alterations in heart rate (RR interval) or other ECG parameters (Figure 6A, Table 2 and Table S4), and did not induce spontaneous arrhythmias: 4 weeks post-infarction only 1 rat in the mock group and 1 rat in the treated group showed ventricular premature beats (16 and 1 premature beats during the ECG recording period, respectively). Our data therefore demonstrate the absence of arrhythmia genesis following injection or implantation of hMuStem cells. Ultrasound studies were performed 1, 3, and 4 weeks post-infarction. As expected, MI induced an increase in LV structural remodeling characterized by an increase in LV chamber dimensions (LVEDD), leading to a decrease in systolic function as evidenced by EF values (Figure 6B, Table 2 and Table S5). Diastolic diameter was increased to 108.93% ± 3.74%, 122.13% ± 5.81%, and 115.20% ± 3.70% of control values, respectively, 1, 3, and 4 weeks post-infarction in rats from the mock group, as compared with 102.23% ± 2.39%, 110.29% ± 4.59%, and 105.64% ± 4.01% of control values in rats from the treated group (Figure 6C and movies S1-S4). Although not significant, these differences suggest that the presence of hMuStem cells results in greater preservation of LVEDD as compared with the mock group. The lack of change in LV wall thickness at the end of diastole was expected at this stage of post-infarction remodeling (first phase of pathological ventricle dilation). While we observed no changes in diastolic function parameters such as the E-wave DT, there was a significant improvement in LV performance in the treated versus the mock group. While EF was reduced to 80.56% ± 2.40%, 70.39% ± 4.53%, and 72.78% ± 3.56% of baseline values, respectively, 1, 3, and 4 weeks post-infarction in rats

from the mock group, the corresponding values in the treated group were 79.88% ± 3.09%, 90.50% ± 3.79%, and 91.10% ± 2.64% (Table 2 and Table S5) (p = 0.0007 and 0.003 at 3 and 4 weeks, respectively; Mann-Whitney test). Overall, these data suggest that hMuStem cell delivery preserves cardiac function.

Discussion

In this study we examined the intramyocardial transplantation of human skeletal muscle-derived MuStem cells in a rat model of MI, in order to assess the feasibility of this approach as a potential advanced therapy medicinal product. Previous preclinical studies have established the ability of MuStem cells to survive in severely damaged tissue, such as dystrophic or cryo-injured skeletal muscle [28,32,44]. Moreover, we have previously demonstrated that MuStem cells can generate significant and persistent clinical and tissue benefits in the GRMD dog model of Duchenne Muscular Dystrophy [28,32,44]. In the present study, we provide original data demonstrating the reparative potential of this adult stem cell population in the context of MI, highlighting its potential for use in regenerative medicine for muscle diseases. We successfully demonstrate that hMuStem cell administration in the border zone of the infarct area is associated with the persistence of this cell population within the injured heart, attenuation of adverse LV tissue remodeling, and an improvement in cardiac function during the next three weeks. Angiogenesis and neo-myogenesis were the main factors that contributed to preservation of the architecture of the LV myocardium.

The number of hMuStem cells injected into sites surrounding the infarct area was less than 3 million, a lower number than that injected in previously published studies [45,46] and expected in the clinic [47–49]. Nonetheless, 9 to 15 tens of thousands of hMuStem cells were detected in each recipient animal 3 weeks after transplantation, indicating a remarkable retention rate. These data distinguish hMuStem cells from MSCs and genetically engineered myoblasts, which are characterized by poor viability in the harsh environment of the damaged myocardium [5,25,50,51]. This suggests that hMuStem cells are less sensitive to the hypoxia and oxidative stress typical of the infarct site. It should be noted that the sensitivity of these cells to the inflammatory response characteristic of MI could not be evaluated in the present study, given that the animal model used was immunodeficient.

Half of the hMuStem cells that engrafted into the infarct area generated predominantly skeletal fibers, possibly reflecting their pre-transplantation specification. Far fewer frequent fibers displayed a cardiac phenotype. This finding is consistent with the very limited contribution of bone marrow (BM) MSCs to cardiac muscle cells following transplantation in a mouse model of acute MI, in which less than 0.1% of grafted cells expressed specific cardiac markers [19]. Although scarce, the presence of muscle fibers expressing the human cardiac marker TNNI indicates an intrinsic potential of hMuStem cells to commit to the cardiomyogenic lineage, in line with previous studies describing the oligopotent nature of these cells [32,33]. A study in which BM-MSCs were stimulated with a cardiopoietic cytokine cocktail before endomyocardial delivery in MI patients reported a 7% increase in LVEF, as compared with 0.2% for non-stimulated cells [52]. In line with this observation and given the potential of hMuStem cells to differentiate into cardiac cells, it may be interesting to further investigate the consequences of *in vitro* preconditioning of these cells. A little over half of the donor nuclei were detected in tissue other than skeletal or cardiac fibers or myofibroblasts, with a location in the collagen matrix 3 weeks after transplantation. This indicates that a large proportion of the hMuStem cells that survived in infarcted tissue did not directly differentiate but instead adopted an interstitial location. Interestingly, we previously described this behavior in hMuStem cells injected into cryo-injured skeletal muscle in immunodeficient mice [32]. These observations are also consistent with those of Quevedo *et al.* (2009), who found that 76% of MSCs were located within the interstitial compartment several weeks after transendocardial injection in a pig model of MI [53]. Those MSCs were smaller than CMs, and did not show a cardiogenic phenotype, evoking an immature state.

Arrhythmogenesis is a major risk associated with the use of stem cell-based therapies in heart diseases. Several serious ventricular arrhythmic events including tachycardia, bradycardia, and bigeminy have been described following administration of murine MDSCs in a mouse model of chronic MI [54]. Similar results were reported after transplantation of hESC-derived CMs into non-human primate models of MI, in which significant ventricular arrhythmias were detected [55]. Interestingly, in

the present study the implantation and subsequent persistence of hMuStem cells in the heart was not associated with any arrhythmias or cardiac electrical alterations other than those caused by the infarct. The absence of arrhythmias may be at least partially explained by the small number of newly formed CMs. Another potential explanation is that donor cell-derived CMs were implanted into the conjunctive matrix, preventing close contact with host CMs and consequent alterations in their electrical properties.

The infarct zone in hMuStem-cell-treated rats was characterized by the presence of many human fast and slow skeletal fibers as well as human $TNNI^+$ fibers, which limited the formation of fibrotic scar tissue. It is tempting to speculate that the formation of these new muscle fibers, although mainly of skeletal origin, may have a more beneficial effect on LV remodeling than fibrous scar tissue, allowing mechanical stabilization of the weakened myocardium. In keeping with this idea, the use of acellular epicardial patches have shown therapeutic efficacy, increasing the mechanical integrity of damaged rat LV tissues [56,57]. A key finding of the present study is the preservation of LVEF 3 weeks after hMuStem cell transplantation into the border region of the infarct. The presence of differentiated cells could promote healing of the infarcted region by maintaining greater elasticity of the ventricular wall, thereby facilitating long-term preservation of function, which in turn may be associated with a reduction in the LV dilation characteristic of scar formation in MI. Consistent with these findings, the functional benefit of MSC therapy appeared to be much greater than that expected based on the observed rate of engraftment [58]. Given the limited number of human $TNNI^+$ fibers detected in the host myocardium, this outcome cannot be attributed to the acquisition of a cardiac phenotype by hMuStem cells. Our findings are in agreement with those of Oshima *et al*. (2005), who also reported a positive functional effect in mouse model of MI despite a low incidence of cardiac phenotype acquisition [24].

Intramyocardial delivery of hMuStem cells promoted marked angiogenesis by increasing capillary density in both central and border zones of the infarct, likely directly contributing to structural and functional recovery. These observations are in agreement with the increased microvascular density

observed within the infarct and peri-infarct area after human pericyte transplantation in a mouse model of acute MI [18]. Interestingly, microRNA-138 (mir-138) increases angiogenesis associated with infarct repair following adventitial progenitor cell transplantation [59]. Moreover, MSC-derived exosomal mir-21 has been shown to increase the expression of angiogenic proteins in a rat model of MI [60], while delivery of adipose MSC-derived exosomes to the peri-infarct area promotes angiogenesis in a mouse model of ischemic heart disease [61]. Further studies of the miRNA secreted by hMuStem cells will be required to better understand the underlying mechanism of action.

One approach to treat MI is to open the artery as soon as possible after the onset of symptoms. The experimental model that best replicates this approach is the ischemia reperfusion model. However, in this scenario angioplasty becomes impossible if the intervention is not sufficiently prompt or if coronary obstruction prevents the passage of a catheter. These clinical cases may require cell injection as soon as possible after MI to promote regeneration or at least preserve function in the injured areas of cardiac muscle. Our permanent ligation model with a short delay of 4 weeks post-MI therefore has clinical relevance. However, despite routine use of this protocol in the laboratory, the LVEF decrease has never exceeded a mean of 20% one week after LAD ligation. These values are likely related to the attenuated inflammatory response in this rat model. Given that cardiac muscle and the associated vasculature receive considerable damage in MI, the LV remodeling observed in our model is particularly relevant, confirming the anti-apoptotic activity of hMuStem cells on host CMs and a pro-angiogenic effect. Moreover, this global beneficial impact on tissue organization was observed after administration of a very small number of hMuStem cells, suggesting that an even greater effect could be obtained by injecting a larger number of cells or by administering a concomitant injection of hMuStem cell secretome. Over the past decade, it has become increasingly apparent that paracrine factors associated and delivered by several types of stem cells are responsible for most of the beneficial effects observed after cell transplantation rather than the cell engraftment and the direct tissue repair [62–65]. Thus, it may be informative to determine the tissue and functional impacts generated by the cell-free

supernatant in the case of the hMuStem cells to clarify to what extent it recapitulates the therapeutic effect of the parent cells. The use of immunodeficient rats is one aspect of the present study that limits our understanding of the behavior and actions of hMuStem cells in damaged heart tissue in the context of MI. Indeed, due to the immunodeficient nature of these rats we could not investigate the immunological component that is yet a key determinant of the post-transplantation survival, recruitment, and function of donor cells with notably a major role of inflammatory cells [5,66–68]. Moreover, this immunological response had important consequences for cardiac remodeling, and in particular the critical supportive role of monocytes and/or macrophages in cardiogenesis and tissue repair [69–72]. Another study limitation that should be borne in mind is that we were unable to evaluate the clinical relevance of the beneficial effect of hMuStem cell transplantation on long-term LV remodeling and cardiac function, since our observations were made only 4 weeks after MI induction. Further, more long-term studies will be required to evaluate post-transplantation responses after the initial compensatory phase.

In conclusion, the use of our hMuStem cell transplantation protocol in a rat model of MI demonstrates the ability of these adult stem cells to engraft in the infarcted heart, where they markedly attenuate adverse tissue remodeling by significantly limiting the development of the fibrotic zone and improving the LV performance without inducing rhythmic abnormalities. These findings pave the way for a potential expansion of the clinical applications of hMuStem cells in the treatment of heart diseases.

Materials and Methods

Human skeletal muscle tissue

Four *Paravertebralis* muscle biopsies were collected from patients aged 12-19 years. Patients were free of known muscle disease and underwent surgery for acute scoliosis at the Department of Pediatric Surgery of the *Centre Hospitalier Universitaire (CHU) de Nantes* (France). Written informed consent was obtained from all patients. All protocols were approved by the Clinical Research Department of the CHU (Nantes, France), according to the rules of the French Regulatory Health Authorities (approval number: MESR/DC-2010-1199). The biological sample bank was created in compliance with national guidelines regarding the use of human tissue for research (approval number: CPP/29/10).

Animals

Immunodeficient *Rag1* and *Il2rg* knockout (KO) Sprague-Dawley rats (RRG rats) [42] were obtained from platform TRIP (Nantes, France) and housed in a controlled environment (temperature 21±1°C, 12-h light/dark cycle) in the specific pathogen-free animal facilities at the IRS-UN (Nantes, France). All efforts were made to minimize suffering. All animals were provided with environmental enrichment: provision of rolls is reported to potentially modify the behavior of housed animals and reduce chronic pain. In addition, suitable end points that were sufficiently predictive and early enough to minimize pain were rigorously applied. At the end of the study, all rats were euthanized by intravenous administration of sodium pentobarbital (300 mg, Dolethal, Vetoquinol SA, Magny Vernois).

A total of 29 rats were included in this study. Animals were subdivided into three groups of sufficient size to provide adequate statistical power. To minimize the number of animals used, several analyses were carried out using the same animals. Animals of the different groups were progressively included in order to be able to anticipate any procedural dysfunction. Two groups each consisted of 10 rats in which infarction was induced by coronary ligation (see "Coronary artery ligation" section below for

description of the procedure), and treated with vehicle (mock group) or hMuStem cells (treated group), respectively (see Table S3). The last group (sham group) consisted of 9 rats undergoing the same surgical procedure than the previous groups but without coronary ligature. Rats from this group were all injected with hMuStem cells. All experimental procedures involving animals were carried out in strict accordance with European Union Directive 2010/63/EU on the protection of animals used for scientific purposes, and were authorized by the French Ministry of Higher Education and Research after approval by the Ethics Committee on Animal Experimentation from the *Pays de la Loire* region (approval number: APAFIS 9573-2017041311597719).

Isolation and culture of hMuStem cells

hMuStem cells were independently isolated from skeletal muscle from 4 patients free of known muscle disease, as previously described [33]. Cells were expanded under standard conditions (37°C in a humidified atmosphere containing 5% CO_2) in growth medium (GM; Macopharma, Mouvaux, France) supplemented with 10% human serum (EFS, Nantes, France), 1% 10,000 IU/mL penicillin, 10 mg/mL streptomycin, 25 µg/mL fungizone (PSF; Sigma-Aldrich, Saint Quentin-Fallavier, France), 10 ng/mL human recombinant basic fibroblast growth factor (bFGF; Miltenyi, Bergisch Gladbach, Germany), and 25 ng/mL human recombinant epidermal growth factor (EGF; Miltenyi). Cells were seeded on CELLstart™ substrate-coated plastic flasks (Invitrogen, Cergy-Pontoise, France) at 1.0-1.5 × 10^4 cells/cm^2 and GM was replaced every 4 days.

Flow cytometry

Cultured hMuStem cell samples (n = 4; P5 corresponding to 10.4-12.7 population doublings) were resuspended in cold PBS/2% human serum and 1.0 × 10^5 cells were incubated (30 min, 4°C in darkness) with fluorochrome-conjugated antibodies (Abs) against the appropriate cell surface marker at saturating concentration (Table S6). Isotype-matched Abs and fluorescence minus control samples

were used as negative controls for gating and analyses. Where applicable, 7-amino-actinomycin D (7-AAD; BD Biosciences, Franklin Lakes, NJ, USA) was added to evaluate cell viability. Samples were acquired using a FACS Aria flow cytometer (BD Biosciences) and data were analyzed using FlowJo software (FlowJo, Ashland, OR, USA). For each labeling experiment, at least 15×10^3 viable cells were considered.

Reverse transcription PCR

Total RNA was extracted from dry pellets of 10^6 cells using the RNeasy mini kit following the manufacturer's instructions (Qiagen, Santa Clara, CA, USA). After DNase treatment (Ambion, Austin, TX, USA), RNA was quantified using a NanoDrop spectrophotometer (Labtech, Wilmington, DE, USA) and processed for reverse transcriptase as previously described [32]. Real-time PCR reactions were performed with specific Taqman® primers and TaqMan® universal PCR Master Mix (Life Technologies™, Carlsbad, CA, USA) on the CFX96 PCR System (BioRad, Marnes La Coquette, France). Data were normalized using HPRT1 as an internal control and differential expression was calculated using the ΔCt method. The oligonucleotide primers used are listed in Table S7.

Western Blotting

Proteins were extracted from 1 x 10^6 cell pellets generated from primary culture of hMuStem cells, myoblasts and glioblastoma cells that were lysed in RIPA buffer (30 min, 4° C). Then, samples were centrifuged at 10,000 g (10 min, 4° C) and protein concentration on supernatants was determined using a BCA protein assay (Sigma-Aldrich, Saint Quentin-Fallavier, France). Fifty µg of proteins were resolved by sodium dodecyl sulfate polyacrylamide gel electrophoresis (SDS-PAGE) on 12 % polyacrylamide gels (Invitrogen, Carlsbad, CA, USA) and electroblotted onto nitrocellulose membranes (Protran BA 83, GE Healthcare, Chicago, IL, USA) using a Bio-Rad® liquid blotting system at 300 mA for 2 h. The membranes were blocked using 50 % Blocking Buffer (Odyssey®, Li-

Cor Biosciences, Lincoln, NE, USA) in PBS (1 h, RT) and incubated (2 h, RT) with primary antibodies against Cx43 (1:5000; C6219, Sigma-Aldrich) and loading control GAPDH (1:1000; Sc25778; Santa Cruz, Dallas, TX, USA). After washing with Tween 0.1 % in PBS, the blots were incubated with AlexaFluor®780-conjugated anti-rabbit secondary antibody (1:10000; A11369; Invitrogen). Equal protein loading was checked through GAPDH labeling and Ponceau S staining of the membranes. The western blot bands were scanned and analyzed with Odyssey®.

Coronary artery ligation

MI was induced by ligation of the LAD coronary artery. Briefly, female RRG rats were anesthetized with a mix of inhaled 3% isoflurane/97% oxygen and subcutaneously injected with 0.1 mg/kg buprenorphine (Buprecare®), after which the chest was shaved. Half of the buprenorphine dose was injected 15 minutes before beginning surgery, and the remainder when the animal awoke. A subcutaneous injection of 1% lidocaine (Xylocaïne) was administered at each cutaneous incision point. Post-operative analgesia (0.1 mg/mL buprenorphine, SC) was maintained for 3-6 days as needed. Animals were then intubated and ventilated using a Harvard Rodent Ventilator (Harvard Apparatus, Les Ulis, France). The tidal volume was 2.5 mL and the respiratory rate was 63 breaths/min. Animals were placed in a supine position on a heating pad. A left lateral thoracotomy at the fourth intercostal space exposed the anterior surface of the heart, after which the location of the LAD coronary artery on the surface of LV anterior wall was identified. The proximal LAD coronary artery was ligated and occlusion was confirmed by observation of a color change and akinesia of the affected area of LV wall. The lungs were expanded before the chest was closed to avoid pneumothorax. To locate and quantify infarction, the wall motion score index was calculated based on echocardiography measurements taken 7 days after MI. M-mode acquisitions were performed in parasternal incidence (short axis) at the base, in the middle, and at the apex of the LV. Systolic function was further assessed by calculation of the LVEF using averaged measurements from 3-5 consecutive cardiac cycles according to the American

Society of Echocardiography guidelines to exclude rats without significant MI (defined as animals with LVEF loss < 15% and an absence of qualitative loss of their wall motion score index). Next, animals were randomized and underwent intramyocardial administration of either buffer only (mock group) or hMuStem cell suspension (treated group). Each group consisted of 10 animals. Importantly, LV dimensions and functional parameters measured at the day 7 follow-up analysis did not significantly differ between the mock and treated groups. Sham-operated rats underwent the same surgical procedure without the coronary ligation (the thread was only passed under the LAD).

Intramyocardial injection of hMuStem cells

Seven days after MI, rats underwent a second open-chest surgery under anesthesia, using the same conditions as described above. Cell layers of hMuStem cell-derived primary cultures (n = 4, independent batch) were dissociated and the cells pelleted and resuspended at 15×10^6 cells/mL in 0.9% NaCl/2.5% homologous serum/10 IU/mL heparin. A volume of 180 µL of suspension (corresponding to 2.7×10^6 cells containing equal contributions from each cell batch) was injected at 6 sites in the border zone of the infarct using a 1-mL syringe with a 27-gauge needle. As described above, a second injection of an analgesic was administered after the animal awoke and before it was placed in the incubator.

Echocardiography

Rats underwent 2-dimensional (2-D) echocardiography using a Vivid 7 Dimension ultrasound system (GE Healthcare, Chicago, IL, USA). Body temperature was maintained at 37°C with a heating pad (Harvard Apparatus) and ECG was monitored during measurements. Anesthesia was induced using 4% isoflurane (Abbott Laboratories, Chicago, IL, USA) and maintained with 2.5% isoflurane during recording. Caution was taken not to apply excessive pressure to the chest, which could cause bradycardia and deformation of the heart. To detect possible structural remodeling, LV diameter and

free-wall thickness were measured from short- and long-axis images obtained by M-mode echocardiography. Systolic function was further assessed by calculation of LVEF using averaged measurements from 3-5 consecutive cardiac cycles in accordance with the guidelines of the American Society of Echocardiography. Left ventricular end-diastolic and end-systolic volumes (LVEDV and LVESV, respectively) were calculated from bi-dimensional short-axis parasternal views taken through the infarcted area by means of the single-plane area-length method. These indexes were calculated in accordance with the standard, widely accepted formulas [73]. Transmitral flow measurements of ventricle filling velocity were obtained with pulsed Doppler, using an apical 4-chamber orientation. Doppler-derived mitral deceleration time, isovolumic relaxation time, E wave, A wave, and the E/A ratio were determined to assess diastolic dysfunction. To avoid bias, experiments were performed and the data analyzed by investigators blind to treatment. Echocardiography measurements were performed 1 day before induction of MI (baseline) to rule out any initial functional differences, after which the MI was induced. Three and 4 weeks after MI induction, ultrasound was also used to assess the consequences of hMuStem cell delivery.

Electrocardiography

For ECG, rats were anaesthetized for with isoflurane as described above. Body temperature was maintained at 37°C with a heating pad (Harvard Apparatus). Using a computer attached to an analog-digital converter IOX 1.585, 6-lead ECG recordings were taken using 25-gauge subcutaneous electrodes (EMKA Technologies, Paris, France) and later analyzed with ECG Auto v3.2.0.2 (EMKA Technologies). ECG parameters were measured on lead II. As described above for echocardiography, ECG measurements were taken 1 day before induction of MI (baseline) to rule out any initial functional differences, and again 4 weeks after the induction of MI to assess the consequences of hMuStem cell delivery.

Histopathological evaluation

Four weeks after MI induction, rats were sacrificed by intravenous administration of sodium pentobarbital (300 mg, Dolethal). After gross examination, the heart, lungs, liver, spleen, kidney, brain, and *Biceps femoris* muscle were sampled to examine the fate of the hMuStem cells in the infarcted heart. The heart was weighed and the tibial bone measured. Next, the heart was divided into 7-8 sections using a rat heart slicer matrix (Zivic Instruments, Pittsburgh, PA, USA). The odd sections were frozen and 10-µm-thick serial sections were cut for immunolabeling and histo-enzymological assays. The even sections were fixed in 10% neutral buffered formalin and embedded in paraffin wax, and 5 µm-thick sections cut and routinely stained with hematoxylin-eosin-saffron (HES) for histopathological evaluation. Additional sections were stained with Picrosirius red stain for collagen. A skilled pathologist certified by the European College of Veterinary Pathology recorded all lesions.

Immunohistochemistry

The frozen sections were first permeabilized (30 min, room temperature [RT]) using 0.1% Triton X-100 (Sigma-Aldrich), incubated (30 min, RT) in blocking buffer (10% goat serum in 0.1 M phosphate-buffered saline [PBS]; Sigma-Aldrich) and incubated overnight at 4°C with the following primary Abs: mouse monoclonal IgG2ak anti-PCNA (1:1000, M0879, Dako, Glostrup, Denmark); Alexa® red 555-conjugated wheat germ agglutinin (1:500, W32464, Invitrogen); mouse monoclonal IgG2b anti-lamin A/C (1:100, MA3-1000, Invitrogen); mouse monoclonal IgG1 anti-skeletal fast myosin (1:400, M4276, Sigma-Aldrich); rabbit polyclonal anti-TNNT1 (1:500, HPA058448, Ozyme SAS, St Quentin Yvelines, France); rabbit monoclonal IgG2b anti-cardiac troponin I (1:250, Ab52852, Abcam, Cambridge, UK); and rabbit polyclonal anti-von Willebrand factor (1:1000, Ab6994, Abcam). Next, the appropriate Alexa® red 555 or green 488 secondary antibodies (1:300, A11008; A21127; A21434, Invitrogen, Carlsbad, CA, USA) were added for 1 hour at RT after which the nuclei were counterstained with DAPI. For immunoperoxidase revelation, sections were incubated with

biotinylated secondary Abs (1:300, E433; E432, Dako) in PBS with 5% rat serum for 1 hour. Bound Abs were detected with streptavidin (P397; Dako) and DAB Liquid Substrate (Dako). Acquisitions were performed under a confocal laser microscope (LSM 780, Zeiss, Oberkochen, Germany) using ZenBlack software (Zeiss) or under a slide scanner (Zeiss Axio Scan Z1, Zeiss). To assess apoptosis in the infarcted heart, TUNEL staining was performed using the Kit Click-iT® Plus TUNEL Assay (Abcam, Cambridge, UK), following the manufacturer's instructions. Apoptotic cells were scored in 5 randomly selected fields per group under a confocal laser microscope (LSM 780, Zeiss). Lamin A/C$^+$ and differentiated cells were counted in serial sections cut from the apex to the septum of the infarcted hearts (S1, S3, S5, or S1-S5 depending on the rat). All counts were performed in at least 2 sections separated by 100 µm on each slide from each of the rats analyzed (n = 5). The number of differentiated cells was determined by counting the number of fibers expressing the different human-specific antibodies relative to the total number of human cells counted (n = 1754 for the 5 rats analyzed). In both groups, angiogenesis was evaluated as the percentage of the heart section area occupied by vWF immunolabeling in 3 different areas. The same threshold was applied to each image using Fiji software while the vWF$^+$ area and the size of the different vWF$^+$ elements were determined automatically. To evaluate anisocytosis, the minimum Feret diameter (MinFeret; shortest distance between two parallel tangents of the muscle fiber edges) of muscle fibers was determined manually in HES-stained sections.

Histomorphometry

Morphometric analysis was performed using a digital camera (Nikon DXM 1200; Nikon Instruments, Badhoevedorp, the Netherlands) combined with image-analysis software (NIS; Nikon). The quantification and morphometric analyses of the immunolabeled sections were performed blindly at 20× magnification. To evaluate anisocytosis, the MinFeret of the transversal CMs was determined manually. The CM perimeter was identified manually to prevent potential errors. Fiber size was documented by measuring the MinFeret of at least 100 fibers per sample in at least 2 randomly selected

microscopic fields in HES-stained sections. The same operator acquired measurements 5 times in the same sample to test repeatability. Intra-assay variation coefficients were always lower than 10%. Fibrosis was evaluated by determining the ratio of collagen-rich areas (identified using specific Picrosirius staining) to the total muscle area in overall cross section. To this end, the area occupied by collagen labeling was automatically measured using a predetermined threshold in NIS freeware.

PCR detection of human DNA

The Alu sequence remains the marker of choice when assessing the biodistribution of transplanted cells in xenogeneic models, owing to its genomic repetition and species specificity. The human Alu (hAlu) sequence can be amplified and quantified by qPCR from genomic DNA (gDNA) with a high degree of accuracy. gDNA was isolated from frozen samples using the NucleoSpin tissue kit (Macherey-Nagel, Hoerdt, France) following the manufacturer's instructions. PCR reactions were carried out on 0.5 µg of input gDNA. Human Alu-specific oligonucleotide primers were designed using Oligo Primer Analysis Software v.7 (Molecular Biology Insights, Colorado Springs, CO, USA) and synthesized by MWG Operon (Eurofins, Ebersberg, Germany): forward primer, 5′-CATGGTGAAACCCCGTCTCTA-3′; reverse primer, 5′-GCCTCAGCCTCCCGAGTAG-3′; probe, 5'-ATTAGCCGGGCGTGGTGGCG-3'. Primers targeting rat GAPDH were also prepared: forward primer, 5′-GAACATCATCCCTGCATCCA-3′; reverse primer, 5′-CCAGTGAGCTTCCCGTTCA-3′. PCR amplifications were performed using the following program: initial denaturation (10 min, 95°C) followed by 40 cycles (15 s, 95°C; 1 min, 60°C; and 1 min, 72°C). By generating a scatter plot of the standard concentrations versus the (Ct) values and determining the equation of the best fit line, the number of human cell equivalents in each qPCR well was calculated.

Statistical analysis

Data were reported as the mean ± standard deviation (SD). Statistical analysis was performed in GraphPad Prism software v6.0f (GraphPad Software, La Jolla, CA, USA) using the Mann-Whitney test and 1- or 2-way ANOVA, followed by the Sidak multiple comparison post-hoc test. Differences were considered significant at p-value < 0.05.

Acknowledgments

The authors thank Cindy Schleder and Samuel Fréhel (INRA/Oniris UMR 0703, Nantes, France) for their respective contributions to the qPCR and morphometric assays, and Blandine Lieubeau (IECM, INRA, Oniris, UBL, F-44307, Nantes, France) for the cytometry experiments. We also thank the technical staff of the UTE IRS1-UN animal facility (Nantes, France) and the Therassay core facility (Nantes, France) for providing the ECG recording platform and the ultrasound scanner. We are grateful to Nathalie Gaborit (l'institut du thorax, INSERM, CNRS, Nantes, France) and Jean-Thomas Vilquin (UMRS 974 Sorbonne Université - INSERM - AIM, Paris, France) for helpful discussion that allowed us to improve the manuscript. Thanks also to Chantal Thorin (NP3 unit, Nutrition, Physiopathologie et Pharmacologie, Oniris, Nantes, France) for assistance with the statistical analyses.

Funding: This work was supported by grant "AAP Pari scientifique 2016" from the Région Pays de la Loire and the Bioregate research/education/innovation program (project title, MuSCO; reference number, 34000650), LabCom SOURIRAT Project (ANR-14-LAB5-0008), ''TEFOR'' «Investissements d'Avenir» (ANRIIINSB-0014), and Labex IGO Project «Investissements d'Avenir» (ANR-11-LABX-0016-01). The study was also financed by INRA (KR's team allocation) and the research unit's own funds (2016-2019), and by the annual Inserm allocation to l'institut du thorax (FC's team allocation). AR's academic thesis was financed by the Bioregate program.

Author contributions: AR performed the *in vivo* protocol, collected, assembled, and interpreted all results, and participated in the preparation of the manuscript; GT performed the *in vivo* protocol and the echocardiography analyses, collected and interpreted the results, and participated in the writing of the

manuscript; TL sacrificed the animals, participated in the tissue sampling process, and provided histopathology/histomorphology expertise; IL isolated the hMuStem cell batches, prepared the cell suspensions for transplantation, and performed some of the immunohistochemistry experiments; ML participated in the tissue sampling, generated the histology slides, and performed the immunohistochemistry experiments; AH participated in the *in vivo* experiments, recorded and analyzed the ECGs, and took care of the animals; CB performed the molecular biology experiments; RF provided expertise in confocal microscopy and participated to the histomorphometry analyses; LD provided bio-imaging expertise; SM and IA generated the immunodeficient rat model and provided the immunodeficient rats required for the study; FC, KR, and LG designed the study, wrote the manuscript, and coordinated the research and strategy. All authors read and approved the final manuscript.

Competing interests: The authors declare that they have no competing interests.

References

1. Hansson, EM, Lindsay, ME and Chien, KR (2009). Regeneration Next: Toward Heart Stem Cell Therapeutics. *Cell Stem Cell* **5**: 364–377.
2. Madonna, R, Ferdinandy, P, De Caterina, R, Willerson, JT and Marian, AJ (2014). Recent developments in cardiovascular stem cells. *Circ. Res.* **115**: 71–78.
3. Segers, VFM and Lee, RT (2008). Stem-cell therapy for cardiac disease. *Nature* **451**: 937–42.
4. Beltrami, AP, Barlucchi, L, Torella, D, Baker, M, Limana, F, Chimenti, S, *et al.* (2003). Adult Cardiac Stem Cells Are Multipotent and Support Myocardial Regeneration. *Cell* **114**: 763–776.
5. Wang, B, Zhang, L, Cao, H, Yang, J, Wu, M, Ma, Y, *et al.* (2017). Myoblast transplantation improves cardiac function after myocardial infarction through attenuating inflammatory responses. *Oncotarget* **8**, 68780–68794.
6. Menasché, P, Hagège, AA, Vilquin, J-T, Desnos, M, Abergel, E, Pouzet, B, *et al.* (2003). Autologous Skeletal Myoblast Transplantation for Severe Postinfarction Left Ventricular Dysfunction. *J. Am. Coll. Cardiol.* **41**: 1078–1083.
7. Bel, A, Messas, E, Agbulut, O, Richard, P, Samuel, JL, Bruneval, P, *et al.* (2003). Transplantation of autologous fresh bone marrow into infarcted myocardium: A word of caution. *Circulation* **108**: 247–252.
8. De Silva, R, Raval, AN, Hadi, M, Gildea, KM, Bonifacino, AC, Yu, ZX, *et al.* (2008). Intracoronary infusion of autologous mononuclear cells from bone marrow or granulocyte colony-stimulating factor-mobilized apheresis product may not improve remodelling, contractile function, perfusion, or infarct size in a swine model of large myocardial. *Eur. Heart J.* **29**: 1772–1782.
9. Gnecchi, M, He, H, Noiseux, N, Liang, OD, Zhang, L, Morello, F, *et al.* (2006). Evidence supporting paracrine hypothesis for Akt-modified mesenchymal stem cell-mediated cardiac protection and functional improvement. *FASEB J.* **20**: 661–669.

10. Yang, K, Song, H, He, S, Yin, W, Fan, X, Ru, F, *et al.* (2019). Effect of neuron-derived neurotrophic factor on rejuvenation of human adipose-derived stem cells for cardiac repair after myocardial infarction. *J. Cell. Mol. Med.* **23**: 5981–5993.

11. Bolli, R, Tang, XL, Sanganalmath, SK, Rimoldi, O, Mosna, F, Abdel-Latif, A, *et al.* (2013). Intracoronary delivery of autologous cardiac stem cells improves cardiac function in a porcine model of chronic ischemic cardiomyopathy. *Circulation* **128**: 122–131.

12. Matsuura, K, Honda, A, Nagai, T, Fukushima, N, Iwanaga, K, Tokunaga, M, *et al.* (2009). Transplantation of cardiac progenitor cells ameliorates cardiac dysfunction after myocardial infarction in mice. *J. Clin. Invest.* **119**: 2204–2217.

13. Cheng, K, Ibrahim, A, Hensley, MT, Shen, D, Sun, B, Middleton, R, *et al.* (2014). Relative roles of CD90 and c-Kit to the regenerative efficacy of cardiosphere-derived cells in humans and in a mouse model of myocardial infarction. *J. Am. Heart Assoc.* **3**: 01–10.

14. Richart, A, Loyer, X, Néri, T, Howangyin, K, Guérin, CL, Ngkelo, A, *et al.* (2014). MicroRNA-21 coordinates human multipotent cardiovascular progenitors therapeutic potential. *Stem Cells* **32**: 2908–2922.

15. Romagnuolo, R, Masoudpour, H, Porta-Sánchez, A, Qiang, B, Barry, J, Laskary, A, *et al.* (2019). Human Embryonic Stem Cell-Derived Cardiomyocytes Regenerate the Infarcted Pig Heart but Induce Ventricular Tachyarrhythmias. *Stem Cell Reports* **12**: 967–981.

16. Kawamura, M, Miyagawa, S, Miki, K, Saito, A, Fukushima, S, Higuchi, T, *et al.* (2012). Feasibility, safety, and therapeutic efficacy of human induced pluripotent stem cell-derived cardiomyocyte sheets in a porcine ischemic cardiomyopathy model. *Circulation* **126**: 29–37.

17. Castro, L, Geertz, B, Reinsch, M, Aksehirlioglu, B, Hansen, A, Eschenhagen, T, *et al.* (2019). Implantation of hiPSC-derived Cardiac-muscle Patches after Myocardial Injury in a Guinea Pig Model. *J. Vis. Exp.* **145**: 58810.

18. Chen, CW, Okada, M, Proto, JD, Gao, X, Sekiya, N, Beckman, SA, *et al.* (2013). Human

pericytes for ischemic heart repair. *Stem Cells* **31**: 305–316.

19. Zhang, J, Wu, Y, Chen, A and Zhao, Q (2015). Mesenchymal stem cells promote cardiac muscle repair via enhanced neovascularization. *Cell. Physiol. Biochem.* **35**: 1219–1229.

20. Schmuck, EG, Koch, JM, Hacker, TA, Hatt, CR, Tomkowiak, MT, Vigen, KK, *et al.* (2015). Intravenous Followed by X-ray Fused with MRI-Guided Transendocardial Mesenchymal Stem Cell Injection Improves Contractility Reserve in a Swine Model of Myocardial Infarction. *J. Cardiovasc. Transl. Res.* **8**: 438–448.

21. Menasche, P (2011). Cardiac cell therapy: Lessons from clinical trials. *J. Mol. Cell. Cardiol.* **50**: 258–265.

22. Zeng, L, Hu, Q, Wang, X, Mansoor, A, Lee, J, Feygin, J, *et al.* (2007). Bioenergetic and functional consequences of bone marrow-derived multipotent progenitor cell transplantation in hearts with postinfarction left ventricular remodeling. *Circulation* **115**: 1866–1875.

23. Makkar, RR, Smith, RR, Cheng, K, Malliaras, K, Thomson, LEJ, Berman, D, *et al.* (2012). Intracoronary cardiosphere-derived cells for heart regeneration after myocardial infarction (CADUCEUS): A prospective, randomised phase 1 trial. *Lancet* **379**: 895–904.

24. Oshima, H, Payne, TR, Urish, KL, Sakai, T, Ling, Y, Gharaibeh, B, *et al.* (2005). Differential myocardial infarct repair with muscle stem cells compared to myoblasts. *Mol. Ther.* **12**: 1130–1141.

25. Menasché, P (2004). Myoblast transfer in heart failure. *Surg. Clin. North Am.* **84**: 125–139.

26. Tambara, K, Sakakibara, Y, Sakaguchi, G, Lu, F, Premaratne, GU, Lin, X, *et al.* (2003). Transplanted skeletal myoblasts can fully replace the infarcted myocardium when they survive in the host in large numbers. *Circulation* **108**: 259–263.

27. Fernandes, S, Amirault, JC, Lande, G, Nguyen, JM, Forest, V, Bignolais, O, *et al.* (2006). Autologous myoblast transplantation after myocardial infarction increases the inducibility of ventricular arrhythmias. *Cardiovasc. Res.* **69**: 348–358.

28. Rouger, K, Larcher, T, Dubreil, L, Deschamps, JY, Le Guiner, C, Jouvion, G, *et al.* (2011). Systemic delivery of allogenic muscle stem cells induces long-term muscle repair and clinical efficacy in duchenne muscular dystrophy dogs. *Am. J. Pathol.* **179**: 2501–2518.

29. Robriquet, F, Babarit, C, Larcher, T, Dubreil, L, Ledevin, M, Goubin, H, *et al.* (2016). Identification in GRMD dog muscle of critical miRNAs involved in pathophysiology and effects associated with MuStem cell transplantation. *BMC Musculoskelet. Disord.* **17**: 209–219.

30. Robriquet, F, Lardenois, A, Babarit, C, Larcher, T, Dubreil, L, Leroux, I, *et al.* (2015). Differential gene expression profiling of dystrophic dog muscle after MuStem cell transplantation. *PLoS One* **10**.

31. Lardenois, A, Jagot, S, Lagarrigue, M, Guével, B, Ledevin, M, Larcher, T, *et al.* (2016). Quantitative proteome profiling of dystrophic dog skeletal muscle reveals a stabilized muscular architecture and protection against oxidative stress after systemic delivery of MuStem cells. *Proteomics* **16**: 2028–2042.

32. Lorant, J, Saury, C, Schleder, C, Robriquet, F, Lieubeau, B, Négroni, E, *et al.* (2018). Skeletal Muscle Regenerative Potential of Human MuStem Cells following Transplantation into Injured Mice Muscle. *Mol. Ther.* **26**: 618–633.

33. Saury, C, Lardenois, A, Schleder, C, Leroux, I, Lieubeau, B, David, L, *et al.* (2018). Human serum and platelet lysate are appropriate xeno-free alternatives for clinical-grade production of human MuStem cell batches. *Stem Cell Res. Ther.* **9**: 128–148.

34. Illa, I, Leon-Monzon, M and Dalakas, MC (1992). Regenerating and denervated human muscle fibers and satellite cells express neural cell adhesion molecule recognized by monoclonal antibodies to natural killer cells. *Ann. Neurol.* **31**: 46–52.

35. Alexander, MS, Rozkalne, A, Colletta, A, Spinazzola, JM, Johnson, S, Rahimov, F, *et al.* (2016). CD82 Is a Marker for Prospective Isolation of Human Muscle Satellite Cells and Is Linked to Muscular Dystrophies. *Cell Stem Cell* **19**: 800–807.

36. Uezumi, A, Nakatani, M, Ikemoto-Uezumi, M, Yamamoto, N, Morita, M, Yamaguchi, A, *et al.* (2016). Cell-Surface Protein Profiling Identifies Distinctive Markers of Progenitor Cells in Human Skeletal Muscle. *Stem Cell Reports* **7**: 263–278.

37. Charville, GW, Cheung, TH, Yoo, B, Santos, PJ, Lee, GK, Shrager, JB, *et al.* (2015). Ex vivo expansion and in vivo self-renewal of human muscle stem cells. *Stem Cell Reports* **5**: 621–632.

38. Ganguly, P, El-Jawhari, JJ, Burska, AN, Ponchel, F, Giannoudis, P V. and Jones, EA (2019). The Analysis of In Vivo Aging in Human Bone Marrow Mesenchymal Stromal Cells Using Colony-Forming Unit-Fibroblast Assay and the CD45 low CD271 + Phenotype . *Stem Cells Int.* **2019**: 1–14.

39. Lin, FX, Zheng, GZ, Chang, B, Chen, RC, Zhang, QH, Xie, P, *et al.* (2018). Connexin 43 Modulates Osteogenic Differentiation of Bone Marrow Stromal Cells Through GSK-3beta/Beta-Catenin Signaling Pathways. *Cell. Physiol. Biochem.* **47**: 161–175.

40. Wiesner, M, Berberich, O, Hoefner, C, Blunk, T and Bauer-Kreisel, P (2018). Gap junctional intercellular communication in adipose-derived stromal/stem cells is cell density-dependent and positively impacts adipogenic differentiation. *J. Cell. Physiol.* **233**: 3315–3329.

41. Kostrominova, TY (2011). Application of WGA lectin staining for visualization of the connective tissue in skeletal muscle, bone, and ligament/tendon studies. *Microsc. Res. Tech.* **74**: 18–22.

42. Ménoret, S, Ouisse, LH, Tesson, L, Delbos, F, Garnier, D, Remy, S, *et al.* (2018). Generation of Immunodeficient Rats With Rag1 and Il2rg Gene Deletions and Human Tissue Grafting Models. *Transplantation* **102**: 1271–1278.

43. Creane, M, Howard, L, O'Brien, T and Coleman, CM (2017). Biodistribution and retention of locally administered human mesenchymal stromal cells: Quantitative polymerase chain reaction–based detection of human DNA in murine organs. *Cytotherapy* **19**: 384–394.

44. Lorant, J, Larcher, T, Jaulin, N, Hedan, B, Lardenois, A, Leroux, I, *et al.* (2018). Vascular

Delivery of Allogeneic MuStem Cells in Dystrophic Dogs Requires Only Short-Term Immunosuppression to Avoid Host Immunity and Generate Clinical/Tissue Benefits. *Cell Transplant.* **27**: 1096–1110.

45. Gautam, M, Fujita, D, Kimura, K, Ichikawa, H, Izawa, A, Hirose, M, *et al.* (2015). Transplantation of adipose tissue-derived stem cells improves cardiac contractile function and electrical stability in a rat myocardial infarction model. *J. Mol. Cell. Cardiol.* **81**: 139–149.
46. Sanganalmath, SK and Bolli, R (2013). Cell Therapy for Heart Failure. *Circ. Res.* **113**: 810–834.
47. Xu, J-Y, Cai, W-Y, Tian, M, Liu, D and Huang, R-C (2016). Stem cell transplantation dose in patients with acute myocardial infarction: A meta-analysis. *Chronic Dis. Transl. Med.* **2**: 92–101.
48. Wang, Z, Wang, L, Su, X, Pu, J, Jiang, M and He, B (2017). Rational transplant timing and dose of mesenchymal stromal cells in patients with acute myocardial infarction: a meta-analysis of randomized controlled trials. *Stem Cell Res. Ther.* **8**: 1–10.
49. Martin-Rendon, E, Brunskill, SJ, Hyde, CJ, Stanworth, SJ, Mathur, A and Watt, SM (2008). Autologous bone marrow stem cells to treat acute myocardial infarction: A systematic review. *Eur. Heart J.* **29**: 1807–1818.
50. Menasché, P (2004). Cellular transplantation: hurdles remaining before widespread clinical use. *Curr. Opin. Cardiol.* **19**: 154–161.
51. Taylor, DA, Hutcheson, KA, Kraus, WE, Atkins, BZ, Glower, DD, Hungspreugs, P, *et al.* (1998). Regenerating functional myocardium: Improved performance after skeletal myoblast transplantation. *Nat. Med.* **4**, 929–933.
52. Bartunek, J, Behfar, A, Dolatabadi, D, Vanderheyden, M, Ostojic, M, Dens, J, *et al.* (2013). Cardiopoietic stem cell therapy in heart failure: The C-CURE (cardiopoietic stem cell therapy in heart failURE) multicenter randomized trial with lineage-specified biologics. *J. Am. Coll. Cardiol.* **61**: 2329–2338.

53. Quevedo, HC, Hatzistergos, KE, Oskouei, BN, Feigenbaum, GS, Rodriguez, JE, Valdes, D, *et al.* (2009). Allogeneic mesenchymal stem cells restore cardiac function in chronic ischemic cardiomyopathy via trilineage differentiating capacity. *Proc. Natl. Acad. Sci. U. S. A.* **106**: 14022–14027.

54. Sekiya, N, Tobita, K, Beckman, S, Okada, M, Gharaibeh, B, Sawa, Y, *et al.* (2013). Muscle-derived stem cell sheets support pump function and prevent cardiac arrhythmias in a model of chronic myocardial infarction. *Mol. Ther.* **21**: 662–669.

55. Chong, JJH, Yang, X, Don, CW, Minami, E, Liu, YW, Weyers, JJ, *et al.* (2014). Human embryonic-stem-cell-derived cardiomyocytes regenerate non-human primate hearts. *Nature* **510**: 273–277.

56. Lin, X, Liu, Y, Bai, A, Cai, H, Bai, Y, Jiang, W, *et al.* (2019). A viscoelastic adhesive epicardial patch for treating myocardial infarction. *Nat. Biomed. Eng.* **3**: 632–643.

57. Chi, NH, Yang, MC, Chung, TW, Chou, NK and Wang, SS (2013). Cardiac repair using chitosan-hyaluronan/silk fibroin patches in a rat heart model with myocardial infarction. *Carbohydr. Polym.* **92**: 591–597.

58. Williams, AR, Hatzistergos, KE, Addicott, B, McCall, F, Carvalho, D, Suncion, V, *et al.* (2013). Enhanced effect of combining human cardiac stem cells and bone marrow mesenchymal stem cells to reduce infarct size and to restore cardiac function after myocardial infarction. *Circulation* **127**: 213–223.

59. Katare, R, Riu, F, Mitchell, K, Gubernator, M, Campagnolo, P, Cui, Y, *et al.* (2011). Transplantation of human pericyte progenitor cells improves the repair of infarcted heart through activation of an angiogenic program involving micro-RNA-132. *Circ. Res.* **109**: 894–906.

60. Wang, K, Jiang, Z, Webster, KA, Chen, J, Hu, H, Zhou, Y, *et al.* (2017). Enhanced Cardioprotection by Human Endometrium Mesenchymal Stem Cells Driven by Exosomal MicroRNA-21. *Stem Cells Transl. Med.* **6**: 209–222.

61. Ma, T, Chen, Y, Chen, Y, Meng, Q, Sun, J, Shao, L, *et al.* (2018). MicroRNA-132, delivered by mesenchymal stem cell-derived exosomes, promote angiogenesis in myocardial infarction. *Stem Cells Int.* **2018**.

62. Kervadec, A, Bellamy, V, El Harane, N, Arakélian, L, Vanneaux, V, Cacciapuoti, I, *et al.* (2016). Cardiovascular progenitor-derived extracellular vesicles recapitulate the beneficial effects of their parent cells in the treatment of chronic heart failure. *J. Hear. Lung Transplant.* **35**: 795–807.

63. Khan, M, Nickoloff, E, Abramova, T, Johnson, J, Verma, SK, Krishnamurthy, P, *et al.* (2015). Embryonic Stem Cell-Derived Exosomes Promote Endogenous Repair Mechanisms and Enhance Cardiac Function Following Myocardial Infarction. *Circ. Res.* **117**: 52–64.

64. Vagnozzi, RJ, Maillet, M, Sargent, MA, Khalil, H, Johansen, AKZ, Schwanekamp, JA, *et al.* (2020). An acute immune response underlies the benefit of cardiac stem cell therapy. *Nature* **577**: 405–409.

65. Yin, L, Liu, X, Shi, Y, Ocansey, DKW, Hu, Y, Li, X, *et al.* (2020). Therapeutic Advances of Stem Cell-Derived Extracellular Vesicles in Regenerative Medicine. *Cells* **9**.

66. Perin, EC, Willerson, JT, Pepine, CJ, Henry, TD, Ellis, SG, Zhao, DXM, *et al.* (2012). Effect of transendocardial delivery of autologous bone marrow mononuclear cells on functional capacity, left ventricular function, and perfusion in chronic heart failure: The FOCUS-CCTRN trial. *JAMA - J. Am. Med. Assoc.* **307**: 1717–1726.

67. Zaruba, MM and Franz, WM (2010). Role of the SDF-1-CXCR4 axis in stem cell-based therapies for ischemic cardiomyopathy. *Expert Opin. Biol. Ther.* **10**: 321–335.

68. Malek, S, Kaplan, E, Wang, JF, Ke, Q, Rana, JS, Chen, Y, *et al.* (2006). Successful implantation of intravenously administered stem cells correlates with severity of inflammation in murine myocarditis. *Pflugers Arch. Eur. J. Physiol.* **452**: 268–275.

69. Sica, A and Mantovani, A (2012). Macrophage plasticity and polarization: In vivo veritas. *J.*

Clin. Invest. **122**: 787–795.

70. Lavine, KJ, Epelman, S, Uchida, K, Weber, KJ, Nichols, CG, Schilling, JD, *et al.* (2014). Distinct macrophage lineages contribute to disparate patterns of cardiac recovery and remodeling in the neonatal and adult heart. *Proc. Natl. Acad. Sci. U. S. A.* **111**: 16029–16034.

71. Heidt, T, Courties, G, Dutta, P, Sager, HB, Sebas, M, Iwamoto, Y, *et al.* (2014). Differential contribution of monocytes to heart macrophages in steady-state and after myocardial infarction. *Circ. Res.* **115**: 284–295.

72. DeBerge, M, Yeap, XY, Dehn, S, Zhang, S, Grigoryeva, L, Misener, S, *et al.* (2017). MerTK cleavage on resident cardiac macrophages compromises repair after myocardial ischemia reperfusion injury. *Circ. Res.* **121**: 930–940.

73. Chen, L, Zhang, J, Hu, X, Philipson, KD and Scharf, SM (2010). The Na+/Ca2+ exchanger-1 mediates left ventricular dysfunction in mice with chronic intermittent hypoxia. *J. Appl. Physiol.* **109**: 1675–1685.

Table

Table 1. ECG and echocardiographic parameters measured in rats from the sham group (without inducing infarction) before (baseline) and 3 weeks after myocardial hMuStem cell transplantation (corresponding to 4 weeks after sham procedure).

ECG	**Baseline**	**3 weeks post-transplantation**
Heart rate (bpm)	399.4 ± 41.3	382.2 ± 37.6
P wave (ms)	19.9 ± 2.1	19.4 ± 1.9
PR interval (ms)	48.7 ± 2.8	47.8 ± 4.1
QRS (ms)	20.0 ± 2.2	22.0 ± 2.3
QT interval (ms)	80.3 ± 5.5	77.2 ± 7.2
Echocardiography	**Baseline**	**3 weeks post-transplantation**
Heart rate (bpm)	336 ± 17	369 ± 8
LVEDWT (mm)	1.63 ± 0.07	1.73 ± 0.08
LVEDD (mm)	7.22 ± 0.27	7.43 ± 0.23
Deceleration time (ms)	39 ± 2	44 ± 4
E/A ratio	1.68 ± 0.12	1.50 ± 0.08
IVRT (ms)	27 ± 0.5	26 ± 0.9
Ejection fraction (%)	84 ± 3	87 ± 2

Data are expressed as the mean ± SD. N = 9 animals.

Table 2. ECG and echocardiographic parameters measured before (baseline) and 4 weeks after induction of myocardial infarction (post-MI) in rats injected with either vehicle (mock group) or hMuStem cells (treated group).

	Mock group		**Treated group**	
ECG	**Baseline**	**4 weeks post-MI**	**Baseline**	**4 weeks post-MI**
Heart rate (bpm)	428.9 ± 26.1	394.4 ± 41.4	396.7 ± 35.1	371.5 ± 28.7
P wave (ms)	18.1 ± 2.1	19.4 ± 3.2	19.6 ± 2.9	20.9 ± 6.6
PR interval (ms)	44.8 ± 2.1	46.8 ± 2.1	45.1 ± 4.3	47.9 ± 3.4
QRS (ms)	19.1 ± 1.1	20.5 ± 2.6	20.0 ± 1.6	20.9 ± 6.6
QT interval (ms)	76.0 ± 5.1	78.3 ± 6.8	78.2 ± 5.7	78.5 ± 10.1
Echocardiography	**Baseline**	**4 weeks post-MI**	**Baseline**	**4 weeks post-MI**
Heart rate (bpm)	381 ± 32	371 ± 37	349 ± 62	353 ± 37
LVEDWT (mm)	1.62 ± 0.22	1.63 ± 0.22	1.49 ± 0.37	1.64 ± 0.29
LVEDD (mm)	5.76 ± 0.24	6.62 ± 0.58	6.13 ± 0.45	6.51 ± 0.45
Deceleration time (ms)	39.7 ± 7.2	42.4 ± 7.03	37.4 ± 9.09	42 ± 4.78
E/A ratio	1.38 ± 0.23	1.25 ± 0.25	1.55 ± 0.31	1.60 ± 0.14
IVRT (ms)	24.5 ± 2.01	26.1 ± 1.85	25.8 ± 3.85	25 ± 2.31
Ejection fraction (%)	87.8 ± 6.16	64.3 ± 13.06	86.4 ± 6.65	79.9 ± 6.81

Data are expressed as the mean ± SD. N = 10 animals per group.

Figures

Figure 1. **Cell lineage-specific phenotype of hMuStem cell population.**

(**A**) Representative flow cytometry profiles of hMuStem cells (n = 4 independent batches) cultured in growth medium (passage 5). Expression of markers of myogenic/satellite cells (CD56, CD29, CD82, and CD318), mesenchymal stem cells (CD73, CD90, and CD105), hematopoietic stem cells (CD45), and perivascular cells (CD140b, CD146) was evaluated. Isotype controls and specific signals are shown in white and gray, respectively. **(B)** Expression of transcripts specific to cardiac-lineage markers (*NKX2.5*, *TBX5*, *RYR2*, *SCN5A*, *TNNT2,* and *GJA1 encoding Cx43 protein*) in 4 MuStem cell batches. *HPRT1* was used as a housekeeping gene. **(C)** Representative western blot showing Cx43 protein (encoded by the *GJA1* gene) expression on hMuStem cells compared to myoblasts and glioblastoma cells (positive and negative control, respectively). GAPDH was used as loading control.

Figure 2. Engraftment of skeletal hMuStem cells in the heart of immunodeficient rats.

(A) Schematic representation of the experimental design. **(B)** Frozen cross-sections of recipient heart were co-labeled with specific human lamin A/C Ab and wheat germ agglutinin (WGA). hMuStem cells were predominantly located in the dense connective tissue. Nuclei were counterstained using DRAQ5 (dark blue). Scale bars: 100 μm (B); 10 μm (insert, B) 1 mm (C); and 250 μm (insert, C). **(C)** Representative hematoxylin-eosin-saffron (HES)- and Picrosirius-stained cross-sections of the cardiac injection zone. **(D)** Representative lead II ECG traces and 2-dimensional (2-D) echocardiography and pulsed Doppler images of rats injected with hMuStem cells before (baseline) and 4 weeks after thread passage. M-mode, time-movement mode; LVEDD, left ventricular end diastolic diameter; E/A ratio, early diastolic (E)/late diastolic (A) ratio; DT, deceleration time; IVRT, isovolumetric relaxation time.

Figure 3. Myocardial transplantation of hMuStem cells limits the expansion of the fibrotic compartment.

(A) Schematic representation of the experimental design. **(B)** Representative hematoxylin-eosin-saffron (HES)-stained cross-section of the infarct zone of rats from the mock and treated groups allowing visualization of the fibrotic, border, and viable zones. Scale bars: 100 μm. **(C)** Representative Picrosirius-stained cross-section of the entire heart of rats from the mock and treated groups. Scale bars: 1 mm. **(D)** Quantification of the MinFeret diameter of myofibers comprising the infarct and viable zones in rats from the mock and treated groups. **(E)** Distribution of muscle fibers according to the minimal Feret diameter in the infarct zone of rats from the mock and treated groups. Statistics: Mann-Whitney test and 1-way ANOVA with Sidak post-hoc test were applied for C and D, respectively. n = 5 animals per group; *$p < 0.05$; ***$p < 0.001$.

Figure 4. Myocardial transplantation of hMuStem cells enhances angiogenesis.

(A) Representative cross-sections of recipient hearts (rats from the mock and treated groups are shown in the left and right columns, respectively) following co-immunolabeling with specific Abs against von Willebrand factor (vWF) and wheat germ agglutinin (WGA). Scale bars: 1 mm and 150 μm (insert). **(B)** Quantification of the vWF^+ surface in the infarct, border, and viable zones in rats from the mock and treated groups. Statistics: 2-way ANOVA with Sidak post hoc test. n = 5 animals per group; ***$p < 0.001$; ****$p < 0.0001$.

Figure 5. hMuStem cells persist as viable cells in infarcted tissue and adopt distinct differentiation profiles.

(A) To visualize hMuStem cells in the context of MI, sections were first labeled with specific human lamin A/C Ab and then counterstained with hematoxylin-eosin-saffron (HES). Next, cross-sections were co-immunolabeled with fluorescent Abs against lamin A/C and wheat germ agglutinin (WGA). **(B)** To investigate the fate of the transplanted hMuStem cells, lamin A/C immunolabeling was successively combined with proliferating cell nuclear antigen (PCNA) immunolabeling and terminal dUPT nick end-labeling (TUNEL). **(C)** Quantification of the phenotype of engrafted human cells using fluorescent co-immunolabeling for lamin A/C and either skeletal fast myosin (MHC) isoform **(D)**, skeletal troponin T1 (TNNT1) isoform **(E),** or cardiac troponin I (TNNI) isoform **(F)** to determine the differentiation behavior of the transplanted hMuStem cells. In parallel, recipient heart muscle serial sections were immunolabeled with Abs against each of these human-specific markers and stained with HES. To explore the ability of hMuStem cells to differentiate into myofibroblasts, Abs against lamin A/C and α-smooth muscle actin (α-SMA) were applied to the same sections **(G)**. Co-immunolabeling for human lamin A/C and WGA was performed on longitudinal sections, revealing the presence of fibers inserted into the conjunctive tissue and composed of several human nuclei **(H)**. Nuclei were counterstained with 10 μg/mL DAPI (blue). Scale bars: 200 μm (A, D-F); 25 μm (insert, A); 500 μm (left, B); 20 μm (insert: left, A; D-F); 200 μm (right, B); 50 μm (insert: right, B; H); 80 μm (G); 18 μm (insert, G); and 10 μm (insert, H).

Figure 6. Myocardial transplantation of hMuStem cells results in functional improvements in the infarcted heart. (A) Representative lead I and lead II ECGs of rats from the mock and treated groups before (baseline) and 4 weeks after MI. **(B, C)** Ultrasound readings were taken repeatedly 1, 3, and 4 weeks after MI by 2-dimensional (2-D) echocardiography and pulsed Doppler (M-mode, time movement mode; ESD, end systolic diameter; EDD, end diastolic diameter; LVEF, left ventricle ejection fraction; DT, deceleration time). Statistics: Kruskal-Wallis test; n = 10 animals per group; $***p < 0.001$.

Figure 1

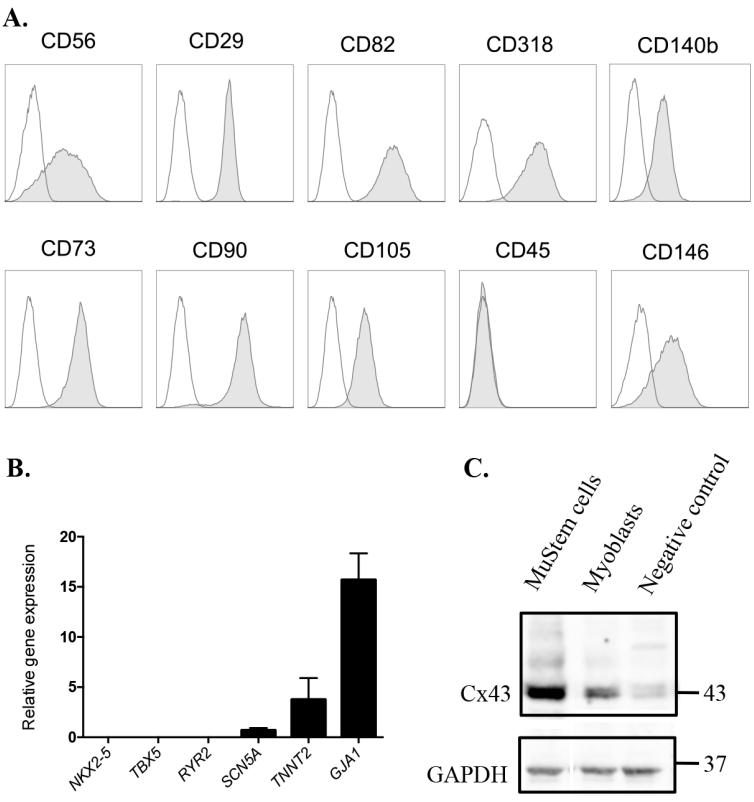
A.
CD56
CD29
CD82
CD318
CD140b
CD73
CD90
CD105
CD45
CD146
B.
Relative gene expression
20
15
10
5
0
NKX2-5
TBX5
RYR2
SCN5A
TNNT2
GJA1
C.
MuStem cells
Myoblasts
Negative control
Cx43
43
GAPDH
37

Figure 2

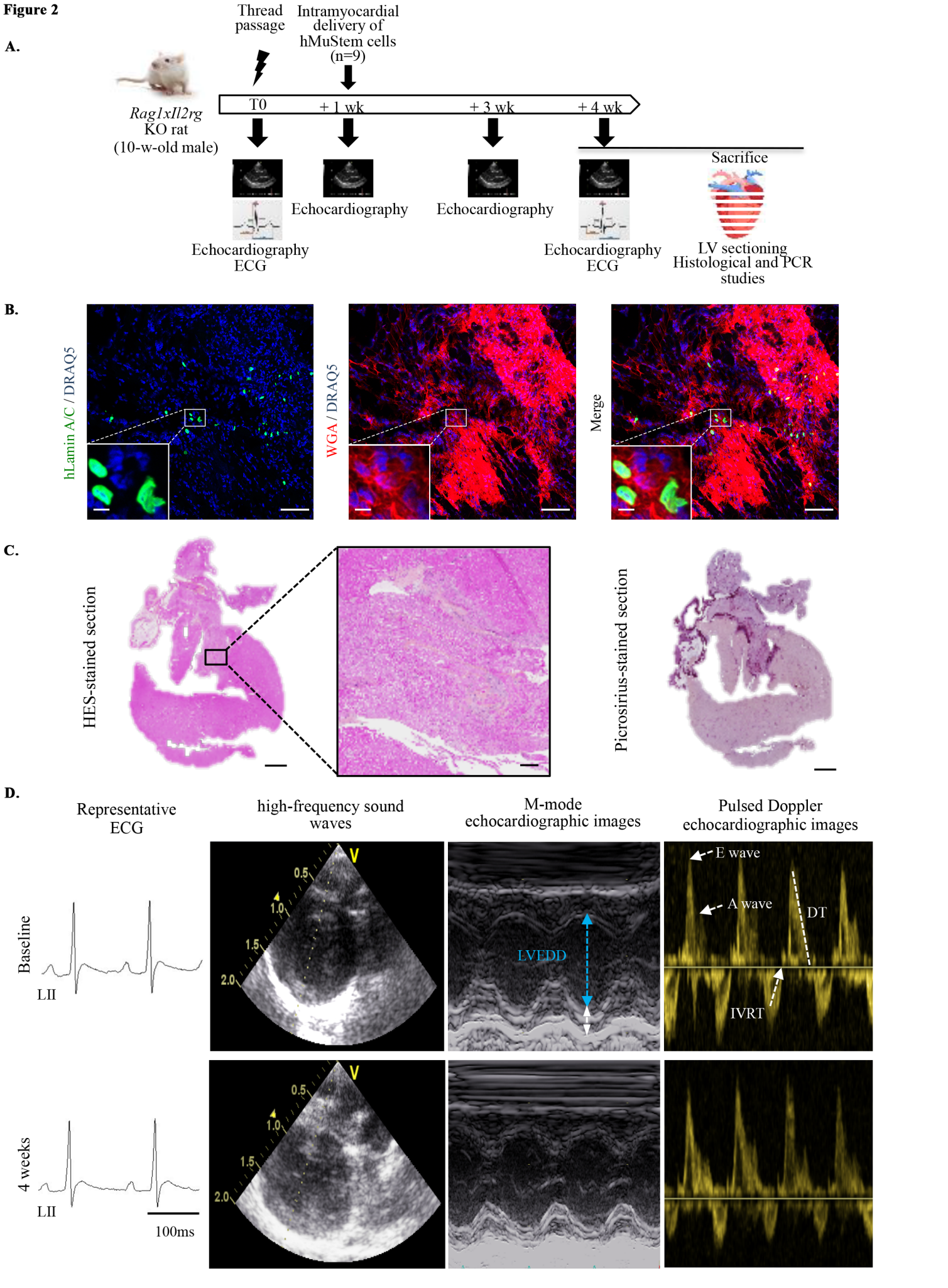
A.
Thread passage
Intramyocardial delivery of hMuStem cells (n=9)
Rag1xIl2rg KO rat (10-w-old male)
T0
+ 1 wk
+ 3 wk
+ 4 wk
Sacrifice
Echocardiography
Echocardiography
Echocardiography ECG
Echocardiography ECG
LV sectioning Histological and PCR studies
B.
hLamin A/C / DRAQ5
WGA / DRAQ5
Merge
C.
HES-stained section
Picrosirius-stained section
D.
Representative ECG
high-frequency sound waves
M-mode echocardiographic images
Pulsed Doppler echocardiographic images
Baseline
LII
4 weeks
LII
100ms
LVEDD
E wave
A wave
DT
IVRT

Figure 3

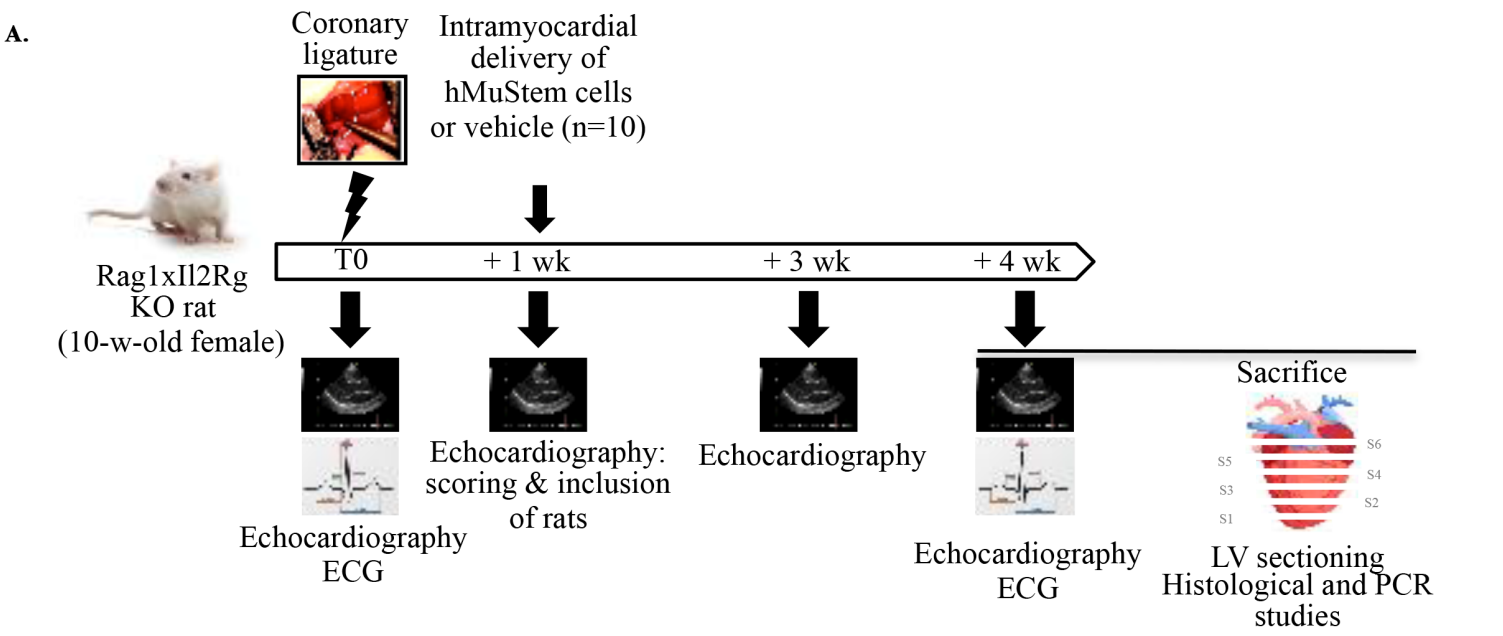
A.
Coronary ligature
Intramyocardial delivery of hMuStem cells or vehicle (n=10)
Rag1xIl2Rg KO rat (10-w-old female)
T0
+ 1 wk
+ 3 wk
+ 4 wk
Echocardiography ECG
Echocardiography: scoring & inclusion of rats
Echocardiography
Echocardiography ECG
Sacrifice
LV sectioning Histological and PCR studies

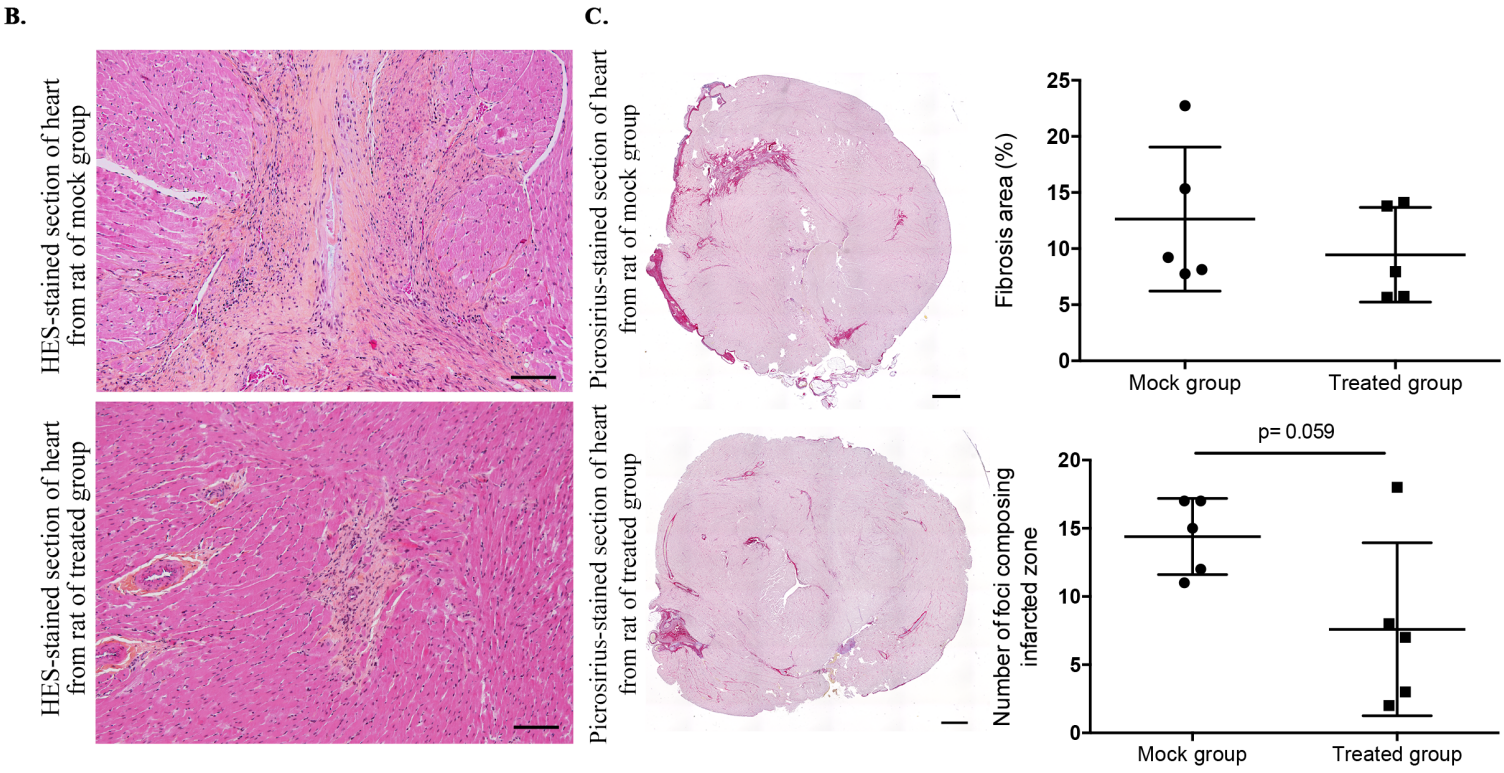
B.
HES-stained section of heart from rat of mock group
HES-stained section of heart from rat of treated group
C.
Picrosirius-stained section of heart from rat of mock group
Picrosirius-stained section of heart from rat of treated group
Fibrosis area (%)
Mock group
Treated group
Number of foci composing infarcted zone
p= 0.059

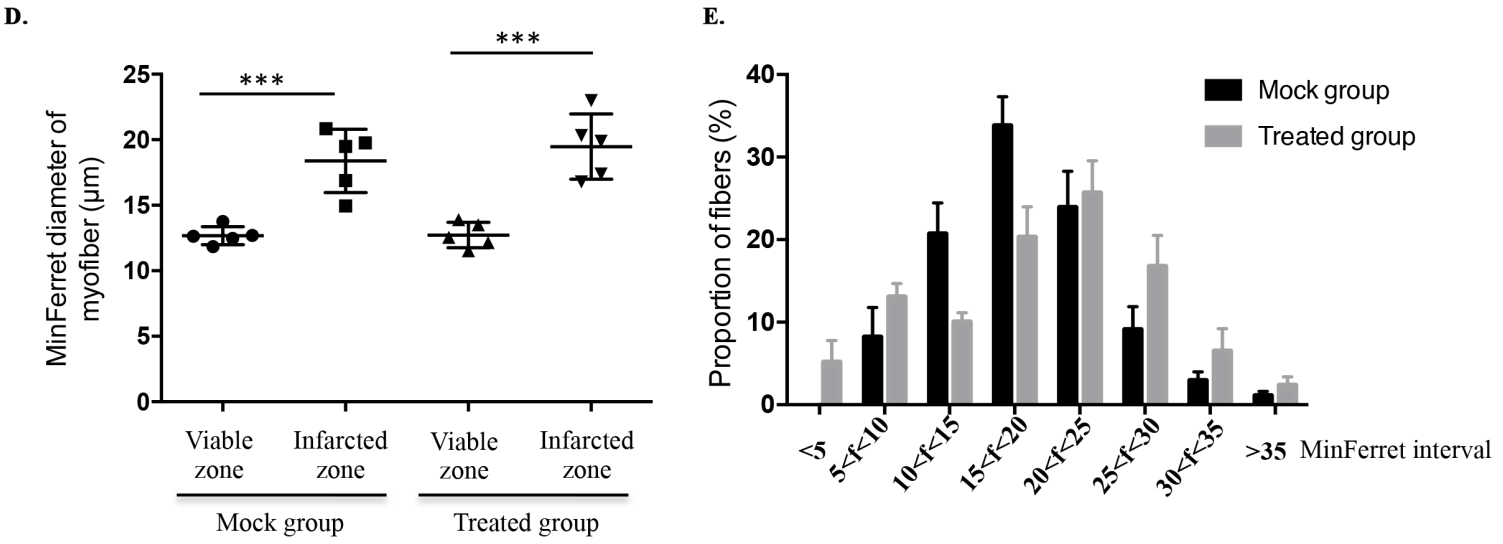
D.
MinFerret diameter of myofiber (µm)
***
***
Viable zone
Infarcted zone
Viable zone
Infarcted zone
Mock group
Treated group
E.
Proportion of fibers (%)
Mock group
Treated group
<5
5<f<10
10<f<15
15<f<20
20<f<25
25<f<30
30<f<35
>35
MinFerret interval

Figure 4

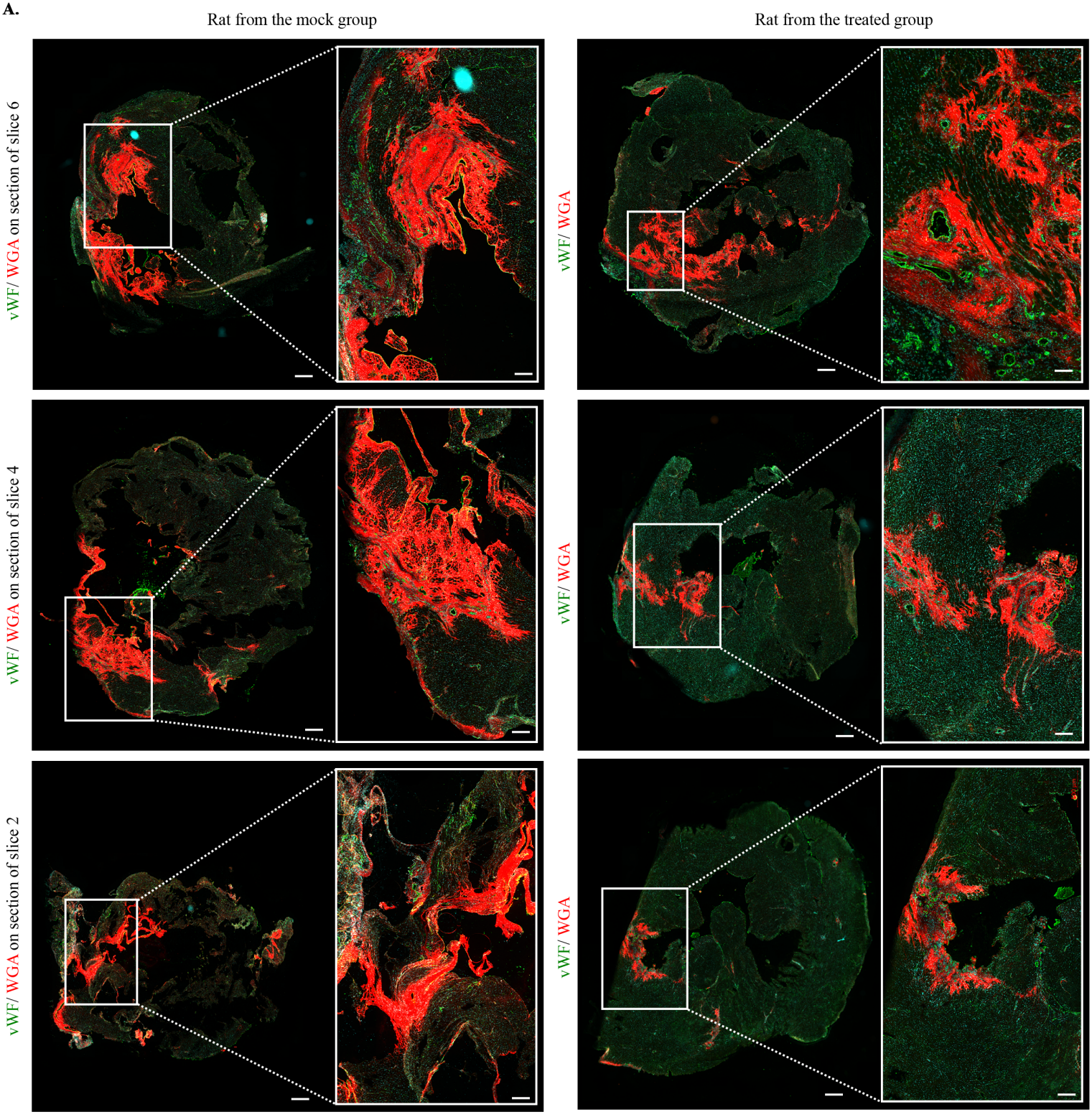
A.
Rat from the mock group
Rat from the treated group
vWF/ WGA on section of slice 6
vWF/ WGA on section of slice 4
vWF/ WGA on section of slice 2
vWF/ WGA
B.
vWF+ surface (%)
40
30
20
10
0
***
***
Mock group
Treated group
Infarcted zone
Border zone
Viable zone

Figure 5

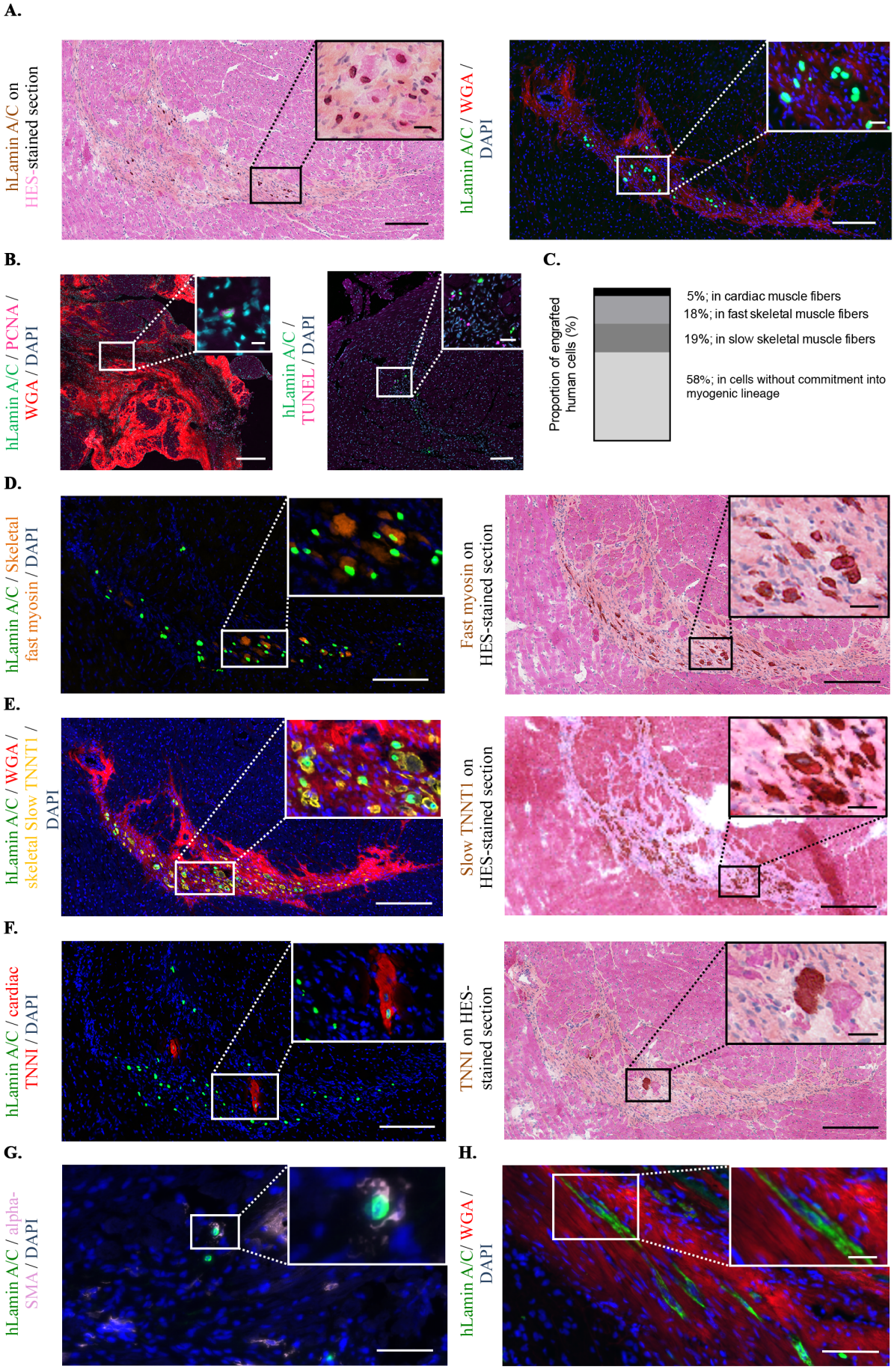
A.
hLamin A/C on HES-stained section
hLamin A/C / WGA / DAPI
B.
hLamin A/C / PCNA / WGA / DAPI
hLamin A/C / TUNEL / DAPI
C.
Proportion of engrafted human cells (%)
5%; in cardiac muscle fibers
18%; in fast skeletal muscle fibers
19%; in slow skeletal muscle fibers
58%; in cells without commitment into myogenic lineage
D.
hLamin A/C / Skeletal fast myosin / DAPI
Fast myosin on HES-stained section
E.
hLamin A/C / WGA / skeletal Slow TNNT1 / DAPI
Slow TNNT1 on HES-stained section
F.
hLamin A/C / cardiac TNNI / DAPI
TNNI on HES-stained section
G.
hLamin A/C / alpha-SMA / DAPI
H.
hLamin A/C/ WGA / DAPI

Figure 6

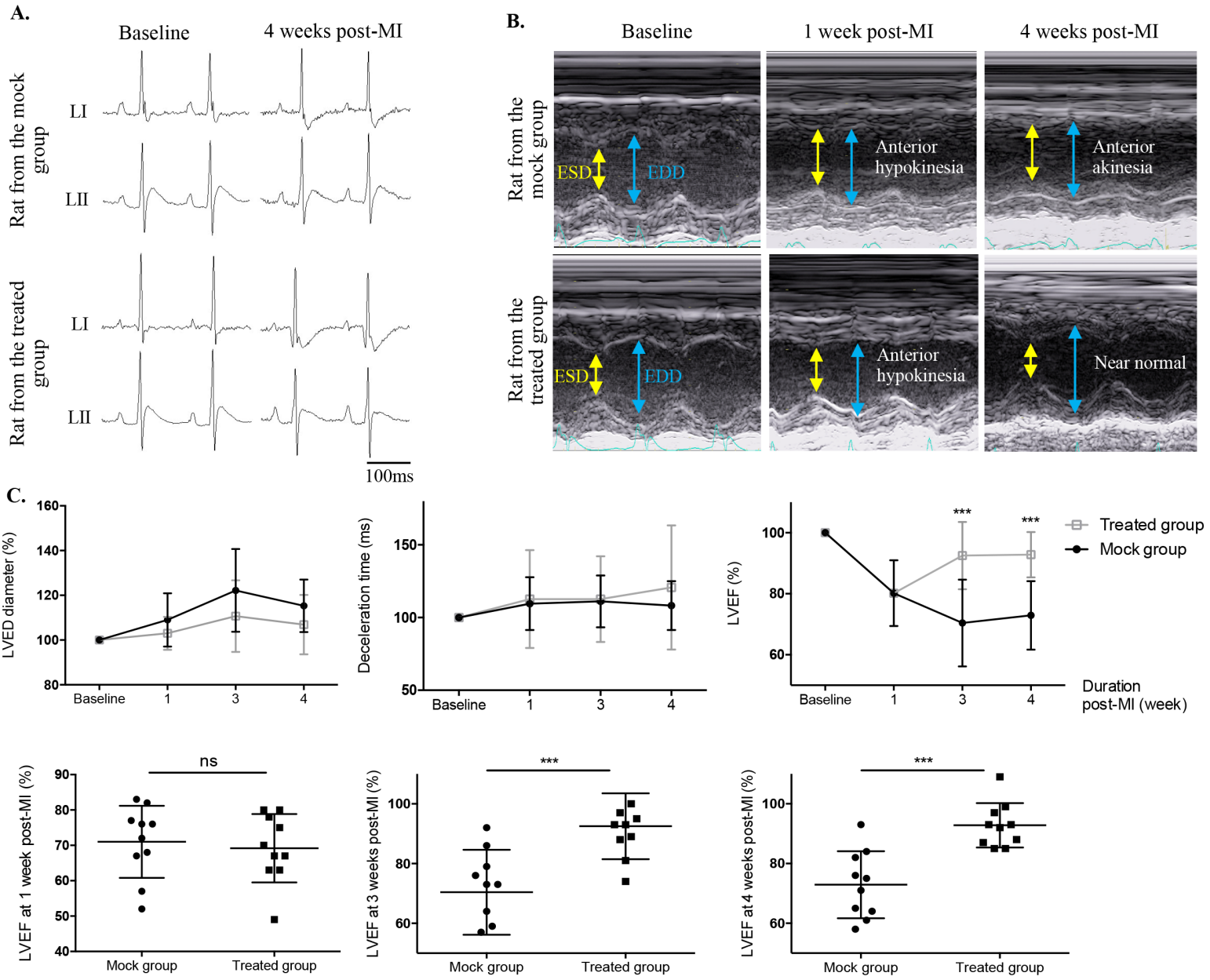
A.
Baseline
4 weeks post-MI
Rat from the mock group
LI
LII
Rat from the treated group
LI
LII
100ms
B.
Baseline
1 week post-MI
4 weeks post-MI
Rat from the mock group
ESD
EDD
Anterior hypokinesia
Anterior akinesia
Rat from the treated group
ESD
EDD
Anterior hypokinesia
Near normal
C.
LVED diameter (%)
Baseline
1
3
4
Deceleration time (ms)
Baseline
1
3
4
LVEF (%)
***
***
Treated group
Mock group
Baseline
1
3
4
Duration post-MI (week)
LVEF at 1 week post-MI (%)
ns
Mock group
Treated group
LVEF at 3 weeks post-MI (%)
***
Mock group
Treated group
LVEF at 4 weeks post-MI (%)
***
Mock group
Treated group

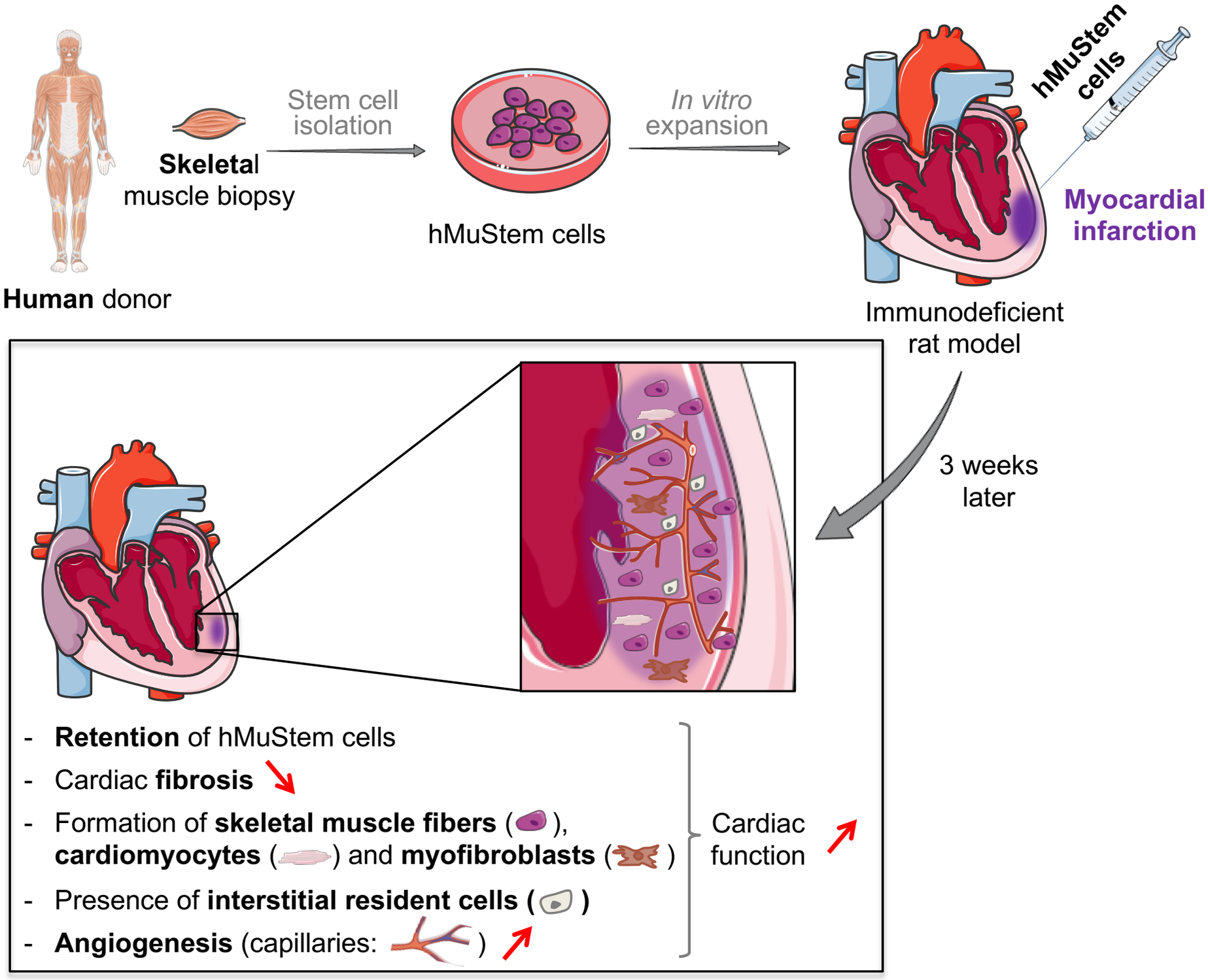
Human donor
Skeletal muscle biopsy
Stem cell isolation
hMuStem cells
In vitro expansion
hMuStem cells
Myocardial infarction
Immunodeficient rat model
3 weeks later
- Retention of hMuStem cells
- Cardiac fibrosis
- Formation of skeletal muscle fibers, cardiomyocytes and myofibroblasts
- Presence of interstitial resident cells
- Angiogenesis (capillaries:
Cardiac function